Homophenylalanine-derived benzo[1,4]diazepine-2,5-diones are strong bacterial quorum sensing inhibitors

Supplementary Information

Manuel Einsiedler,[a,b,†] Sanja Škaro Bogojević,[c,†] Dušan Milivojević,[c] Sandra Vojnović,[c] Miloš K. Milčić,[d] Veselin Maslak,[d] Anke Matura,[b] Tobias A. M. Gulder[a,b,*] and Jasmina Nikodinović-Runić[c,*]

[a] Helmholtz Institute for Pharmaceutical Research Saarland (HIPS), Department of Natural Product Biotechnology, Helmholtz Centre for Infection Research (HZI) and Department of Pharmacy at Saarland University, PharmaScienceHub (PSH), Campus E8.1, 66123, Saarbrücken, Germany. *E-mail: tobias.gulder@helmholtz-hips.de

[b] Chair of Technical Biochemistry, Technische Universität Dresden, Bergstraße 66, 01069 Dresden, Germany. *E-mail: tobias.gulder@tu-dresden.de

[c] Institute of Molecular Genetics and Genetic Engineering, University of Belgrade, Vojvode Stepe 444a, 11042, Belgrade 152, Serbia. *E-mail: jasmina.nikodinovic@imgge.bg.ac.rs

[d] Faculty of Chemistry, University of Belgrade, Studentski trg 12–16, Belgrade 11000, Serbia.

† These authors contributed equally.

Contents

1. General Chemical Methods

Solvents and Reagents

Solvents for HPLC and MS analysis, such as acetonitrile and methanol, were purchased from Fisher Scientific and VWR in purity of over 99% (HPLC-grade). Water was purified using a TKA GenPure water treatment system and deionised. Dry solvents, such as acetonitrile, dichloromethane, methanol, ethanol and tetrahydrofuran, for procedures under an inert atmosphere were prepared by distillation and dried over molecular sieves (3 Å or 4 Å). Commercial materials and other solvents were purchased at the highest commercial quality from the providers Acros Organics, Alfa Aesar, Carbolution, Carl Roth, Merck, Sigma Aldrich, VWR, TCI Chemicals and Thermo Fisher Scientific.

Solid Phase Peptide Synthesis (SPPS)

Fmoc test

A small amount of resin (5 – 10 mg) was deprotected in 1 mL of 20% piperidine in DMF for 20 minutes. The resin was filtered off and 100 µL of the obtained solution was diluted with 10 mL of DMF. Three samples of 1 mL were transferred into cuvettes and the absorbance was measured using a NanoPhotometer® P330 by *Implen*, while DMF was used as a reference. The absorbances were used to calculate the average resin loading via:

$$resin\ loading\ \left[\frac{mmol}{g}\right] = \frac{101 \cdot A_{301nm}}{7.8 \cdot m_{resin}}$$

With A_{301nm}: Absorbance at 301 nm and m_{resin}: mass of used loaded resin in mg.

Chromatography

Thin-layer chromatography (TLC) was performed on precoated plates of silica gel F254 (Merck) with UV detection at 254 and 365 nm. Column chromatography was performed on silica gel 60 Geduran® Si 60 (40-60 µm) (Merck). High Performance Liquid Chromatography (HPLC) analysis was performed on a Knauer system consisting of an UV-1575 Intelligent UV/VIS-Detector, DG-2080-53 3-Line Degasser, two PU-1580 Intelligent HPLC Pumps, AS-1550 Intelligent Sampler, HG-1580-32 Dynamic Mixer and a LC-NetII/ADC. The system was controlled by the Galaxie software. A reversed phase column (100-3 C18 A, 150 × 4.6 mm) with integrated precolumn manufactured by Knauer at 25 °C was used with the following solvents: A = H_2O + 0.05% TFA, B = ACN + 0.05% TFA. The separation method consisted of the following gradient system: 0–2 min: 95% A, 2–25 min: 95–5% A, 25–28 min: 5% A, 28–31 min: 95% A, with a flowrate of 1 mL/min. All traces were monitored at 220 nm. Purification of compounds was performed on a semi-preparative Medium Pressure Liquid Chromatography (MPLC) device (Reveleris X2) manufactured by Grace with reversed phase columns (C18, 12 g). The system was controlled by the Reveleris Navigator software and the eluent system consisted of A and B. The separation method used the following gradient system: 0–2 min: 95% A, 2–21 min: 95–5% A, 21–23 min: 5% A, 23–25 min: 95% A, with a flowrate of 28 mL/min. Preparative HPLC was performed on a Jasco system consisting of an UV-1575 Intelligent UV/VIS-Detector, two PU-2086 Plus Intelligent Prep pumps, MIKA 1000 Dynamic Mixing Chamber, 1000 µL injection port and a LC-NetII/ADC. The system was controlled by the Galaxie software. A reversed phase column (100-5 C18 A, 250 × 16 mm) manufactured by Knauer was used. The separation method consisted of the following gradient system: 0–2 min: 95% A, 2–25 min: 95–5% A, 25–26 min: 5% A, 26–28 min: 95% A. The used flow rate was 12 mL/min at 220 nm.

HR-MS

For high resolution mass spectrometry an Agilent mass spectrometer 6538 with electron spray ionisation (ESI), with high resolution Q-TOF mass analyser and microchannel plate detector was used.

NMR

^{1}H and ^{13}C Nuclear Magnetic Resonance Spectra (NMR) were recorded on Bruker AVANCE 300 and AVANCE 600 spectrometers at 298 K. The chemical shifts are given in δ-values (ppm) and were referenced internally on the residual peak of the deuterated solvent ($CDCl_3$: δ_H = 7.26 ppm; DMSO-d_6: δ_H = 2.50 ppm) and the corresponding carbon peak ($CDCl_3$: δ_C = 77.16 ppm; DMSO-d_6: δ_C = 39.52 ppm), respectively. ^{19}F chemical shifts were internally referenced using residual TFA ($CDCl_3$: δ_F = –75.39 ppm).[1] The coupling constants *J* are given in Hertz [Hz] and determined assuming first-order spin-spin coupling. The following abbreviations were used for the allocation of signal multiplicities: bs – broad singlet, s – singlet, d – doublet, bd – broad doublet, t – triplet, q – quartet, m – multiplet or combinations thereof. In the case of different conformers with a predominant one, only the ^{13}C signals of the major conformer are given.

Specific Rotation

The specific rotation was measured with a PerkinElmer Model 341 LLC Polarimeter at 20 °C in chloroform. The concentration of the compounds during the measurements is given in 10 mg/mL.

2. Bioactivity Assessment

***Pseudomonas aeruginosa* DM50 disc assay:**

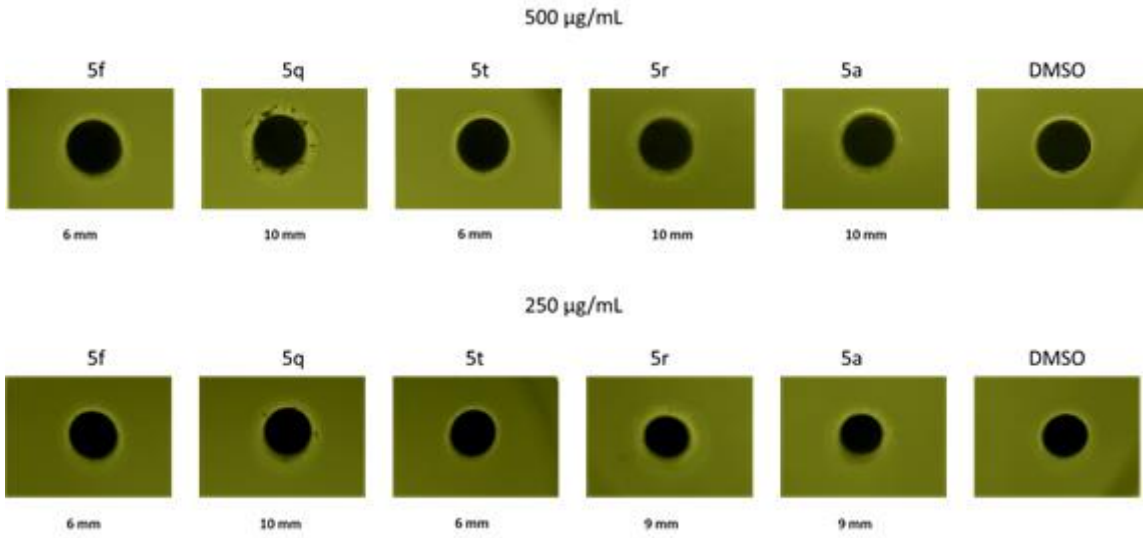

Figure S1. Anti-quorum-sensing activity of benzo[1,4]diazepine-2,5-diones **5f**, **5q**, **5t**, **5r**, **5a** detected by *Pseudomonas aeruginosa* BK25H. The effect of compounds (500 and 250 µg/disc) on pyocyanin production is represented by the diameter of blurry white halos around discs. DMSO is negative control.

***Chromobacterium violaceum* CV026 broth assay:[2]**

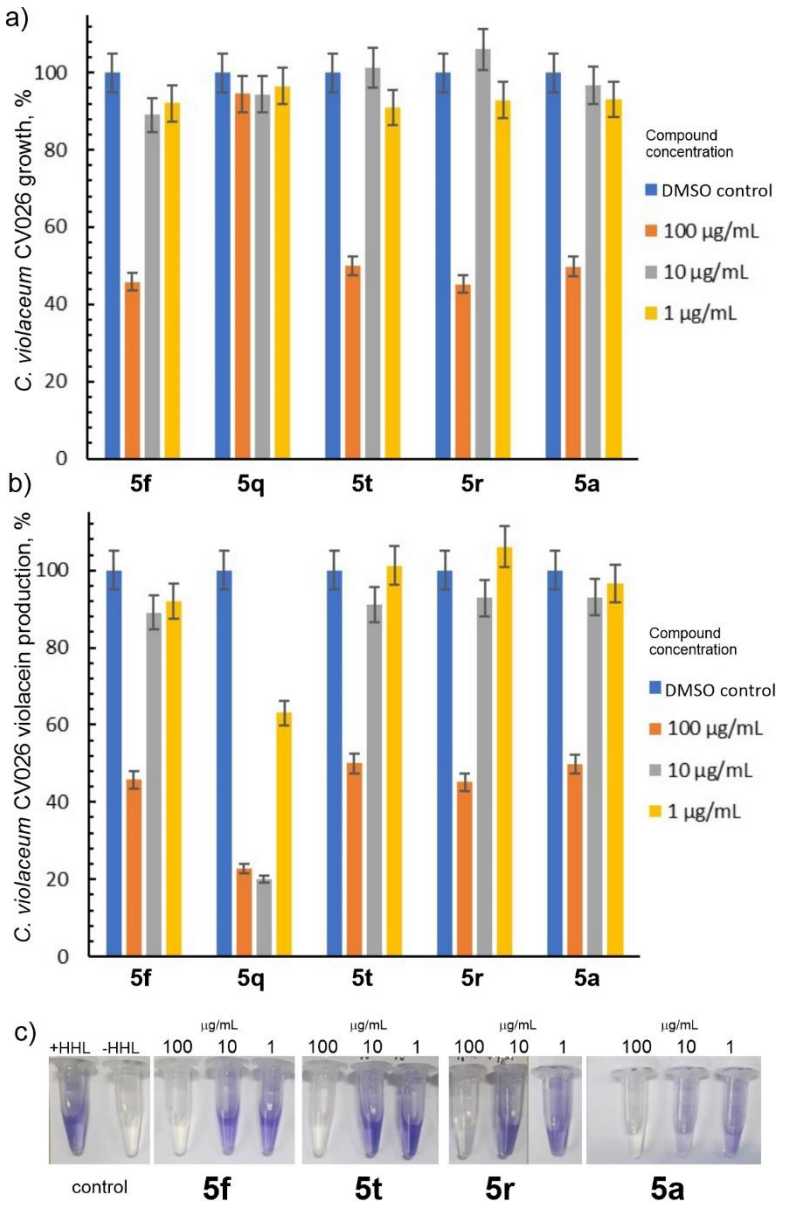

Figure S2. Growth (a) and violacein production (b) of *C. violaceum* CV026 in liquid cultures in the presence of 100, 10 or 1 µg/mL of five best benzo[1,4]diazepine-2,5-diones (**5f**, **5q**, **5t**, **5r**, **5a**) in comparison to untreated controls (DMSO). c) Water-butanol extracts of the corresponding cultures *C. violaceum* CV026 containing **5f**, **5t**, **5r**, **5a**.

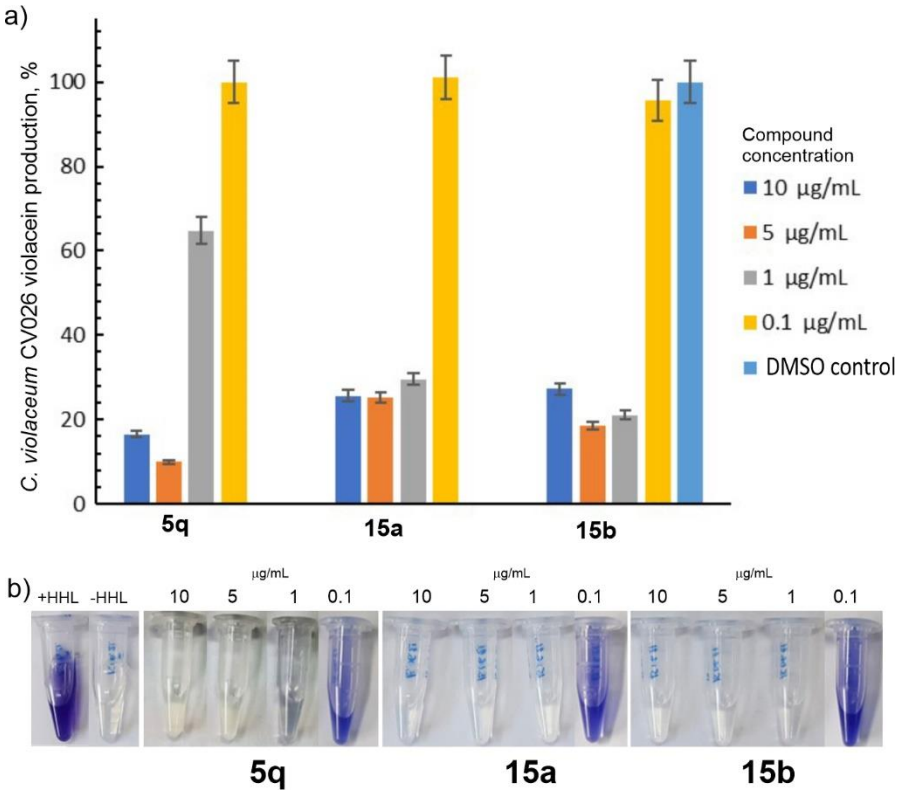

Figure S3. a) Violacein production in *C. violaceum* CV026 liquid cultures in the presence of 10, 5, 1 and 0.1 µg/mL of benzo[1,4]diazepine-2,5-diones **5q**, **15a**, and **15b**. *C. violaceum* CV026 with HHL inducer incubated in LB medium without addition of tested compounds is a control (DMSO control), b) Water-butanol extract of the corresponding cultures.

Cytotoxicity assessment and *C. elegans* toxicity assay:

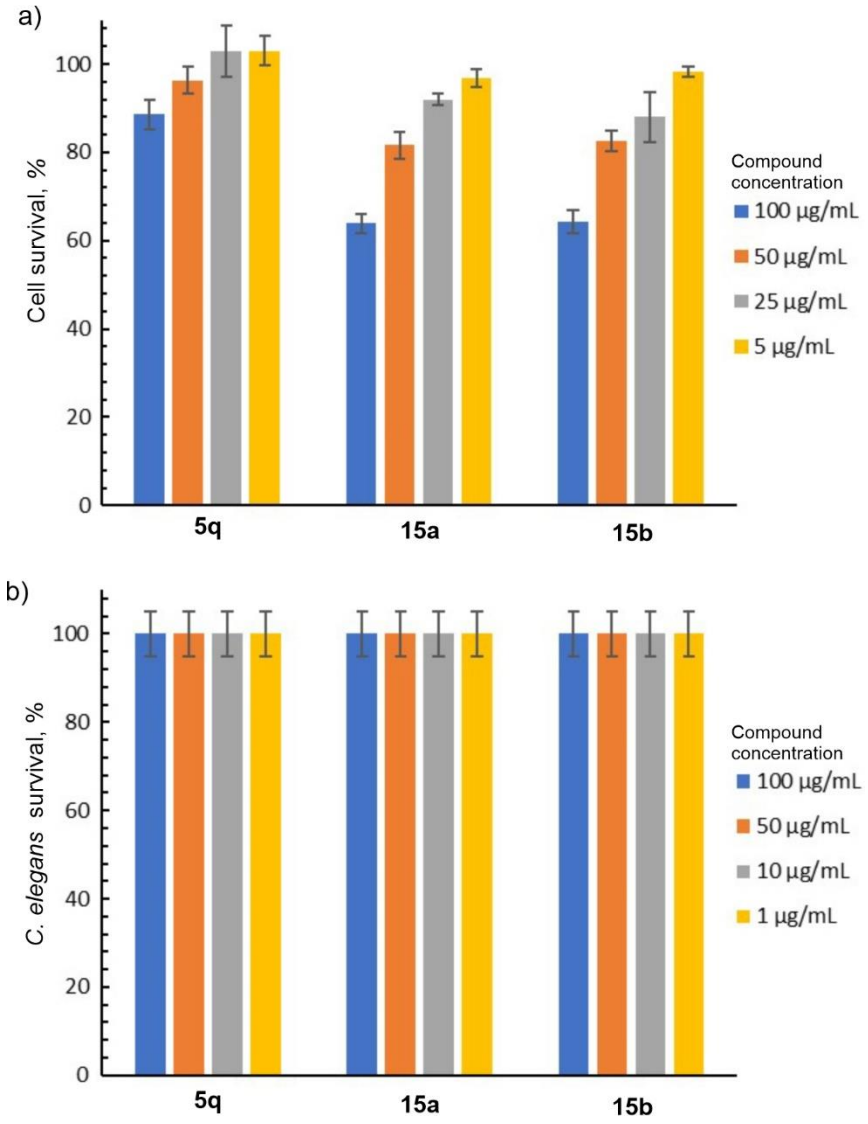

Figure S4. Toxicity of benzo[1,4]diazepine-2,5-diones (**5q**, **15a**, and **15b**) on a) *in vitro* MRC-5 cells, and b) *in vivo C. elegans.*

3. Synthetic Details

All benzo[1,4]diazepine-2,5-diones **5a**–**5q** (except **5a**, **5e** and **5s**, see below) and as well as Fmoc-protected anthranilic acid derivatives **11a** to **11i** used within this study were prepared and characterised as reported in our previous studies on AsqJ and its substrate promiscuity.[3, 4]

(*S*)-3-isobutyl-3,4-dihydro-1*H*-benzo[1,4]diazepine-2,5-dione (**5a**)

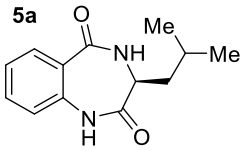

This compound was synthesised starting from (*S*)-Fmoc-leucine and purified by MPLC, yielding 37.0 mg (0.16 mmol, 73%) of a beige solid.

^{1}H-NMR (400 MHz, DMSO-d_6)**:** δ [ppm] = 10.36 (s, 1 H), 8.44 (d, *J* = 5.9 Hz, 1 H), 7.73 (dd, *J* = 7.8, 1.5 Hz, 1 H), 7.51 (dt, *J* = 7.8, 1.5 Hz, 1 H), 7.21 (dt, *J* = 7.6, 1.0 Hz, 1 H), 7.10 (d, *J* = 8.1 Hz, 1 H), 3.60 (q, *J* = 6.5 Hz, 1 H), 1.77–1.62 (m, 1 H), 1.55 (t, *J* = 7.0 Hz, 2 H), 0.84 (d, *J* = 6.6 Hz, 3 H), 0.76 (d, *J* = 6.6 Hz, 3 H).

^{13}C{^{1}H}-NMR (100 MHz, DMSO-d_6)**:** δ [ppm] = 171.7, 167.8, 136.8, 132.3, 130.4, 126.3, 124.0, 121.0, 50.3, 36.2, 24.9, 22.9, 21.6.

HR-MS (ESI+)**:** *m/z* calcd. for $C_{13}H_{16}N_2O_2$ [M+H]$^+$: 233.1285, found: 233.1280.

HPLC: t_R = 8.3 min.

Specific rotation: $[\alpha]_D$ = +113.2 °·mL·dm^{-1}·g^{-1} (ρ = 1.47; MeOH).

(*R*)-3-(*tert*-butoxymethyl)-4-methyl-3,4-dihydro-1*H*-benzo[1,4]diazepine-2,5-dione (**5e**)

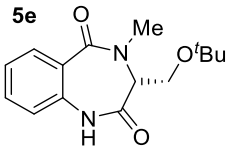

This compound was synthesised starting from (*R*)-Fmoc-(O^{t}Bu)serine, yielding 46.0 mg (0.17 mmol, 41%) of an beige solid.

^{1}H-NMR (600 MHz, $CDCl_3$)**:** δ [ppm] = 8.77 (bs, 0.2 H), 8.48 (bs, 0.7 H), 7.96 (bd, *J* = 7.9 Hz, 1 H), 7.46 (td, *J* = 7.7, 1.6 Hz, 1 H), 7.30–7.23 (m, 1 H)*, 6.99 (bd, *J* = 8.1 Hz, 1 H), 4.25 (bs, 0.2 H), 4.15 (bt, *J* = 7.3 Hz, 0.8 H), 4.02–3.93 (m, 0.8 H), 3.87–3.78 (m, 0.8 H), 3.40–3.25 (m, 1.1 H), 3.18 (s, 2.3 H), 1.21 (s, 7 H), 0.96 (s, 2 H).

* Signal overlaps with solvent residual peak.

^{13}C{^{1}H}-NMR (151 MHz, $CDCl_3$)**:** δ [ppm] = 170.1, 168.5, 135.4, 132.4, 131.8, 127.8, 125.5, 120.7, 74.1, 57.5, 55.9, 28.9, 27.5.

^{1}H NMR showed a mixture of conformers.

HR-MS (ESI+)**:** *m/z* calcd. for $C_{15}H_{20}N_2O_3$ [M+Na]$^+$: 299.1366, found: 299.1365.

HPLC: t_R = 10.2 min.

Specific rotation: $[\alpha]_D$ = –36.5 °·mL·dm^{-1}·g^{-1} (ρ = 0.55; $CHCl_3$).

(*S*)-3-(but-3-en-1-yl)-4-methyl-3,4-dihydro-1*H*-benzo[1,4]diazepine-2,5-dione (**5s**)

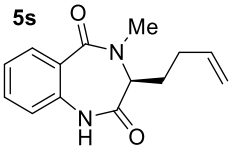

This compound was synthesised starting from (*S*)-Fmoc-homoallylglycine, yielding 86.0 mg (0.35 mmol, 86%) of an orange solid.

^{1}H-NMR (600 MHz, $CDCl_3$)**:** δ [ppm] = 9.59 (s, 0.3 H), 9.36 (s, 0.7 H), 7.89–7.97 (m, 1 H), 7.45 (t, *J* = 6.9 Hz, 1 H), 7.20–7.27 (m, 1 H), 7.04 (d, *J* = 7.6 Hz, 1 H), 5.67–5.77 (m, 0.7 H), 5.57–5.66 (m, 0.3 H), 4.98 (d, *J* = 17.1 Hz, 1.3 H), 4.94 (d, *J* = 10.1 Hz, 0.7 H), 4.03 (t, *J* = 7.4 Hz, 0.3 H), 3.96 (t, *J* = 7.1 Hz), 3.29 (s, 1 H), 3.09 (s, 2 H), 2.09–2.22 (m, 1.3 H), 2.01–2.08 (m, 1.3 H), 1.93–2.00 (m, 0.7 H), 1.53–1.68 (m, 0.7 H).

^{13}C{^{1}H}-NMR (151 MHz, $CDCl_3$)**:** δ [ppm] = 170.7, 168.9, 136.6, 135.8, 132.5, 131.4, 127.4, 125.4, 120.8, 116.2, 54.9, 30.4, 29.2, 25.5.

NMR spectra showed a mixture of conformers. Only the ^{13}C-signals of the major conformer are given.

HR-MS (APCI+)**:** *m/z* calcd. for $C_{14}H_{16}N_2O_2$ [M+H]$^+$: 245.1285, found: 245.1282.

HPLC: t_R = 9.9 min.

Specific rotation: $[\alpha]_D$ = +70.9 °·mL·dm^{-1}·g^{-1} (ρ = 2.15; MeOH).

Synthesis of Fmoc-*N*-Me-L-homophenylalanine (8)

(9*H*-fluoren-9-yl)methyl (*S*)-5-oxo-4-phenethyloxazolidine-3-carboxylate (**7**)[5]

In a flame-dried 250 mL-Schlenk flask, *N*-Fmoc-Homophenylalanine (3.50 g, 8.72 mmol, 1.0 eq.) was dissolved in dry DCM (9 mL/mmol), and paraformaldehyde (2.60 g, 86.6 mmol, 10 eq.) and magnesium sulfate (8 g) were added. The mixture was vigorously stirred and boron trifluoride diethyletherate (1.10 mL, 1.24 g, 8.74 mmol, 1.0 eq.) was added slowly. After stirring under argon for 5 hours, the mixture was filtered and the solids were rinsed with DCM. The combined filtrates were washed with 1 M HCl_{aq} (1 × 25 mL) and brine (1 × 25 mL), dried over Na_2SO_4 and the solvent was removed under reduced pressure. The crude product was purified by column chromatography (pentane/EtOAc = 5/1) to yield the oxazolidinone as 2.57 g (6.22 mmol, 71%) of yellowish oil.

^{1}H-NMR (600 MHz, $CDCl_3$)**:** δ [ppm] = 7.77 (bs, 2 H), 7.57–7.53 (m, 2 H), 7.46–7.27 (m/bs, 6 H), 7.25–6.97 (m/bs, 3 H), 5.53–5.10 (bs, 1 H), 5.01 (s, 1 H), 4.83–4.46 (m/bs, 2 H), 4.33 (bs, 0.4 H), 4.22 (bt, *J* = 5.5 Hz, 1 H), 3.90 (bs, 0.5 H), 2.80–2.11 (bs, 3 H), 2.00–1.71 (bs, 1 H).

^{13}C{^{1}H}-NMR (151 MHz, $CDCl_3$)**:** δ [ppm] = 172.0, 153.0, 143.4 (2C), 141.4 (2C), 140.0, 128.4 (2C), 128.3 (2C), 128.0 (2C), 127.2 (2C), 126.3, 124.5 (2C), 120.1 (2C), 77.8, 67.3, 54.4, 47.1, 31.6, 30.3.

^{1}H NMR showed very broad signals in general. ^{13}C NMR showed a mixture of conformers, only the signals of the major conformer are given.

HR-MS (APCI+)**:** *m/z* calcd. for $C_{26}H_{23}NO_4[M+H]^+$: 414.1700, found: 414.1688.

HPLC: t_R = 15.8 min.

***R*$_f$:** 0.28 (pentane/EtOAc = 5/1).

Specific rotation: $[\alpha]_D$ = +69.0 °·mL·dm^{-1}·g^{-1} (ρ = 6.50; $CHCl_3$).

(*S*)-2-((((9*H*-fluoren-9-yl)methoxy)carbonyl)(methyl)amino)-4-phenylbutanoic acid (**8**)

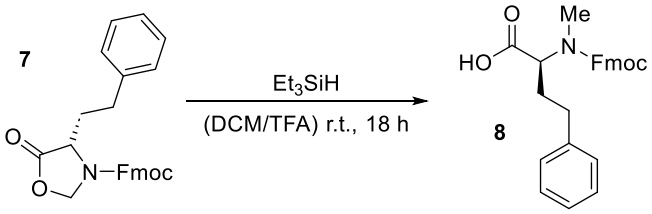

In a 250 mL round-bottomed flask, 5-oxooxazolidinone (2.46 g, 5.95 mmol, 1.0 eq.) was dissolved in DCM and TFA (1/1, 6 mL/mmol), then triethylsilane (3.30 mL, 2.44 g, 21.4 mmol, 3.0 eq.) was added slowly and the resulting mixture stirred at room temperature for 18 hours. The volatiles was removed under reduced pressure and the residue purified by MPLC to yield Fmoc-protected *N*-methylated Homophenylalanine as 2.36 g of a white solid (5.68 mmol, 95%).

^{1}H-NMR (600 MHz, $CDCl_3$)**:** δ [ppm] = 7.78 (dd, *J* = 7.7, 3.0 Hz, 1.2 H), 7.73 (dd, *J* = 7.6, 3.9 Hz, 0.8 H), 7.63 (dd, *J* = 7.6, 4.5 Hz, 1.2 H), 7.51 (dd, *J* = 14.0, 7.5 Hz, 0.8 H), 7.41 (bq, *J* = 7.3 Hz, 1.2 H), 7.38–7.26 (m, 4.5 H), 7.25–7.14 (m, 3.2 H), 4.82 (dd, *J* = 10.7, 4.8 Hz, 0.6 H), 4.57–4.43 (m, 2.4 H), 4.30 (t, *J* = 6.9 Hz, 0.6 H), 4.16 (t, *J* = 6.2 Hz, 0.4 H), 2.91 (s, 1.2 H), 2.88 (s, 1.8 H), 2.70–2.56 (m, 1.6 H), 2.50–2.43 (m, 0.4 H), 2.40–2.31 (m, 0.6 H), 2.26–2.19 (m, 0.4 H), 2.14–2.05 (m, 0.6 H), 1.99–1.90 (m, 0.4 H).

^{13}C{^{1}H}-NMR (151 MHz, $CDCl_3$)**:** δ [ppm] = 177.0, 157.3, 143.9 (2C), 141.5 (2C), 140.7, 128.6 (2C), 128.5 (2C), 127.9 (2C), 127.2 (2C), 126.4, 125.2 (2C), 120.1 (2C), 68.0, 58.6, 57.4, 32.6, 31.0, 30.4.

NMR spectra showed a mixture of conformers. Only the ^{13}C signals of the major conformer are given.

HR-MS (APCI+)**:** *m/z* calcd. for $C_{26}H_{25}NO_4$ $[M+Na]^+$: 438.1676, found: 438.1674.

HPLC: t_R = 15.1 min.

Specific rotation: $[\alpha]_D$ = –4.9 °·mL·dm^{-1}·g^{-1} (ρ = 0.67; MeOH).

Loading of Amino Acid on Wang Resin[3]

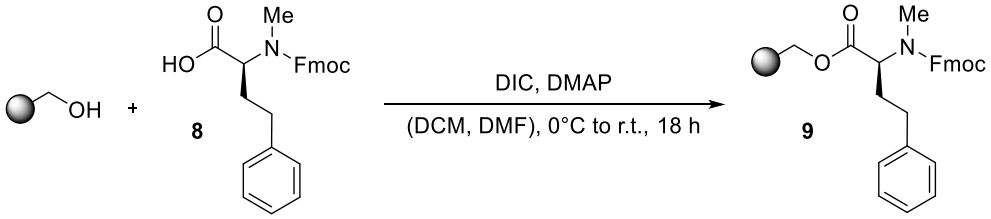

In an SPPS reactor, dry DCM was added to Wang resin (1.1 mmol/g, 1.0 eq.) and shaken for 30 minutes. In a flame-dried Schlenk flask the Fmoc-protectedhomophenylalanine (1.2 eq.) was dissolved in a mixture of DCM and DMF (7:1, 5 mL/mmol acid) and the solution cooled to 0 °C. *N*,*N*'-diisopropylcarbodiimide (DIC, 5.0 eq.) was slowly added, followed by the addition of *N*,*N*-dimethylaminopyridine (DMAP, 0.1 eq.). The solution was stirred at 0 °C for 2 minutes, added to the swollen resin, and vigorously shaken for 18 h at room temperature. Afterward, the solution was removed, and the resin was washed with DMF (3 × 5 mL), MeOH (3 × 5 mL) and DCM (4 × 5 mL). After drying the resin *in vacuo*, loading was determined using the Fmoc-test. Loading was 0.6 mmol/g.

Capping was achieved by adding a mixture of pyridine (2.0 eq.) and acetic anhydride (2.0 eq.) in 6 mL of DCM to the resin and shaking for 15 minutes. The resin was washed with DCM (4 × 5 mL).

Fmoc Deprotection

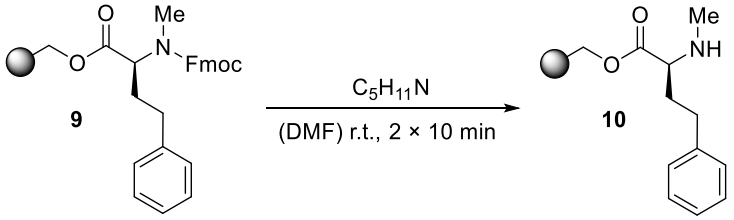

The resin was washed with DMF (5 mL). Next, the resin was treated with piperidine (20% v/v in DMF) and shaken for 15 minutes. The procedure was repeated once, then the resin was washed with DMF (3 × 5 mL), MeOH (3 × 5 mL) and DCM (4 × 5 mL).

Coupling with Functionalised Fmoc-protected Anthranilic Acids

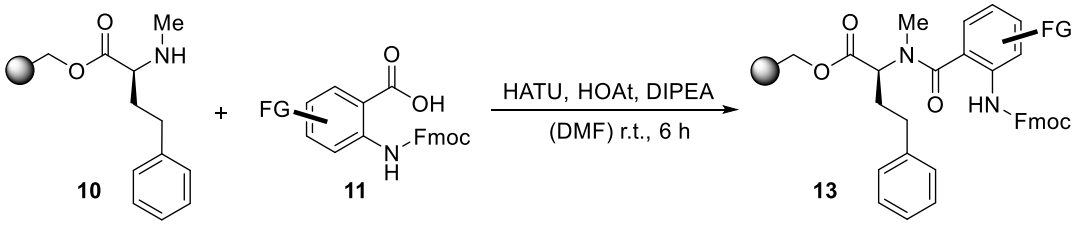

The resin was washed with DMF (5 mL). In a 10 mL round bottomed flask, (functionalised) *N*-Fmoc-benzoic acid (1.3 eq.), HATU (2.0 eq.), HOAt (2.0 eq.) and DIPEA (4.0 eq.) were dissolved in DMF (2 mL). After the addition of this solution to the resin, it was shaken for 6 hours. Afterward, the resin was washed with DMF (3 × 5 mL), MeOH (3 × 5 mL) and DCM (4 × 5 mL).

Fmoc Deprotection of Dipeptide

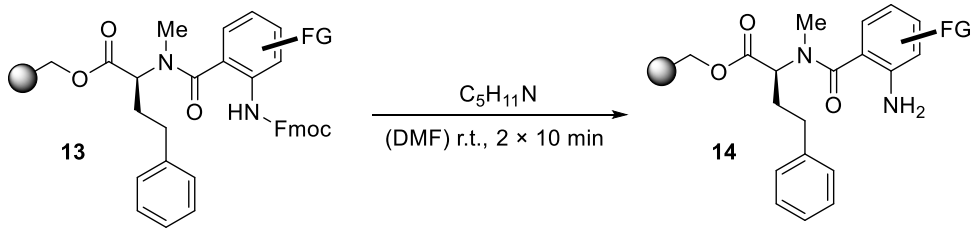

The second Fmoc deprotection was carried out in the same way as described above.

Cyclisation to Benzo[1,4]diazepine-2,5-diones[6]

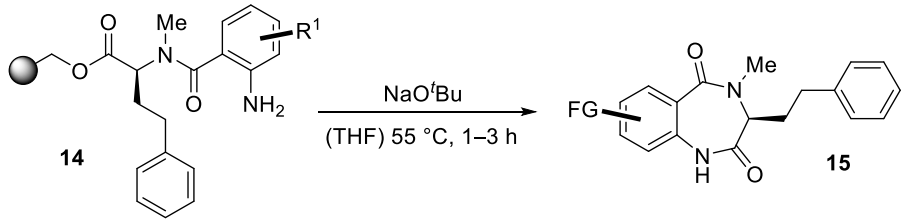

The resin was dried *in vacuo* and suspended in THF, sodium *tert*-butoxide (2.0 eq.) was added and the mixture was heated to 50 °C under an argon atmosphere. After completion of the reaction monitored by HPLC, the resin was filtered off and washed with methanol (3 × 5 mL). The solvent of the combined filtrates was removed under reduced pressure before being purified by preparative HPLC.

(*S*)-6-fluoro-4-methyl-3-phenethyl-3,4-dihydro-1*H*-benzo[1,4]diazepine-2,5-dione (**15a**)

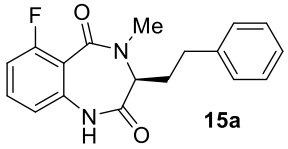

This compound was obtained as 41.8 mg of a white solid (134 µmol, 70%).

^{1}H-NMR (600 MHz, $CDCl_3$)**:** δ [ppm] = 9.17 (bs, 1 H), 7.40–7.34 (m, 1 H), 7.27–7.22 (m, 2.1 H)*, 7.19–7.13 (m, 2.6 H), 7.05–6.94 (m, 1.3 H), 7.86–7.80 (m, 1 H), 4.06–3.99 (m, 1 H), 3.22 (s, 0.4 H), 3.11 (s, 2.6 H), 2.71–2.55 (m, 2 H), 2.36–2.28 (m, 0.9 H), 2.25–2.17 (m, 0.9 H), 1.94–1.87 (m, 0.1 H), 1.86–1.78 (m, 0.1 H).

* Signal overlaps with solvent residual peak.

^{13}C{^{1}H}-NMR (151 MHz, $CDCl_3$)**:** δ [ppm] = 170.7 (d, *J* = 6.4 Hz), 164.6, 161.8 (d, *J* = 256 Hz), 140.2, 137.3, 132.6 (d, *J* = 10.4 Hz), 128.7 (2C), 128.5 (2C), 126.6, 116.8 (d, *J* = 15.1 Hz), 116.4, 113.1 (d, *J* = 22.2 Hz), 54.7, 32.4, 28.4, 28.1.

^{19}F{^{1}H}-NMR (282 MHz, $CDCl_3$)**:** δ [ppm] = –109.0 (s, 0.1 F), –109.3 (s, 0.9 F).

NMR spectra showed a mixture of conformers. Only the ^{13}C signals of the major conformer are given.

HR-MS (ESI+)**:** *m/z* calcd. for $C_{18}H_{17}FN_2O_2$ $[M+Na]^+$: 335.1166, found: 335.1167.

HPLC: t_R = 10.8 min.

Specific rotation: $[\alpha]_D$ = +121.9 °·mL·dm^{-1}·g^{-1} (ρ = 1.05; $CHCl_3$).

(*S*)-7-fluoro-4-methyl-3-phenethyl-3,4-dihydro-1*H*-benzo[1,4]diazepine-2,5-dione (**15b**)

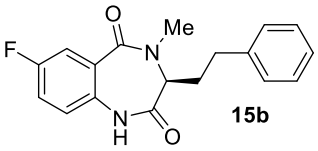

This compound was obtained as 14.7 mg of a yellowish solid (47.1 µmol, 25%).

^{1}H-NMR (600 MHz, $CDCl_3$)**:** δ [ppm] = 9.29 (s, 0.3 H), 9.04 (s, 0.7 H), 7.26–7.22 (m, 1.9 H)*, 7.20–7.11 (m, 3.5 H), 7.05–6.97 (m, 1.6 H), 4.05 (bt, *J* = 7.4 Hz, 0.3 H), 3.94 (t, *J* = 7.3 Hz, 0.7 H), 3.25 (s, 0.9 H), 3.12 (s, 2.1 H), 2.73–2.58 (m, 2 H), 2.44–2.36 (m, 0.7 H), 2.22–2.16 (m, 0.7 H), 1.91 (bs, 0.3 H), 1.82 (bs, 0.3 H).

* Signal overlaps with solvent residual peak.

^{13}C{^{1}H}-NMR (151 MHz, $CDCl_3$)**:** δ [ppm] = 170.4, 167.5, 159.7 (d, *J* = 247 Hz), 140.3, 132.0, 129.3 (d, *J* = 7.1 Hz), 128.8 (2C), 128.4 (2C), 126.6, 122.6 (d, *J* = 7.9 Hz), 120.0 (d, *J* = 23.0 Hz), 117.6 (d, *J* = 23.9 Hz), 54.9, 32.6, 29.3, 28.3.

^{19}F{^{1}H}-NMR (282 MHz, $CDCl_3$)**:** δ [ppm] = –115.4 (s, 0.7 F), –116.0 (s, 0.3 F).

NMR spectra showed a mixture of conformers. Only the ^{13}C signals of the major conformer are given.

HR-MS (ESI+)**:** *m/z* calcd. for $C_{18}H_{17}FN_2O_2$ $[M+Na]^+$: 335.1166, found: 335.1164.

HPLC: t_R = 11.0 min.

Specific rotation: $[\alpha]_D$ = +67.3 °·mL·dm^{-1}·g^{-1} (ρ = 0.74; $CHCl_3$).

(*S*)-8-fluoro-4-methyl-3-phenethyl-3,4-dihydro-1*H*-benzo[1,4]diazepine-2,5-dione (**15c**)

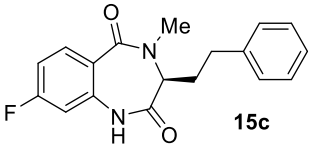

This compound was obtained as 24.2 mg of a yellowish solid (77.4 µmol, 41%).

^{1}H-NMR (600 MHz, $CDCl_3$)**:** δ [ppm] = 9.19 (bs, 0.3 H), 9.01 (bs, 0.7 H), 8.06–7.91 (m, 1 H), 7.25–6.95 (m, 6 H)*, 6.76–6.68 (m, 1 H), 4.05 (bs, 0.3 H), 3.95 (t, *J* = 7.4 Hz, 0.7 H), 3.25 (s, 1 H), 3.12 (s, 2 H), 2.75–2.57 (m, 2 H), 2.44–2.36 (m, 0.7 H), 2.24–2.16 (m, 0.7 H), 1.92 (bs, 0.3 H), 1.84 (bs, 0.3 H).

* Signal overlaps with solvent residual peak.

^{13}C{^{1}H}-NMR (151 MHz, $CDCl_3$)**:** δ [ppm] = 170.5, 168.1, 164.8 (d, *J* = 253 Hz), 140.3, 137.5 (d, *J* = 10.1 Hz), 134.0 (d, *J* = 10.3 Hz), 128.8 (2C), 128.4 (2C), 126.6, 123.9, 113.1 (d, *J* = 21.5 Hz), 107.5 (d, *J* = 24.9 Hz), 55.0, 32.6, 29.3, 28.3.

^{19}F{^{1}H}-NMR (282 MHz, $CDCl_3$)**:** δ [ppm] = –105.7 (bs, 0.3 F), –105.8 (bs, 0.7 F).

NMR spectra showed a mixture of conformers. Only the ^{13}C signals of the major conformer are given.

HR-MS (ESI+)**:** *m/z* calcd. for $C_{18}H_{17}FN_2O_2$ $[M+Na]^+$: 335.1166, found: 335.1170.

HPLC: t_R = 11.0 min.

Specific rotation: $[\alpha]_D$ = +60.0 °·mL·dm^{-1}·g^{-1} (ρ = 0.72; $CHCl_3$).

(*S*)-9-fluoro-4-methyl-3-phenethyl-3,4-dihydro-1*H*-benzo[1,4]diazepine-2,5-dione (**15d**)

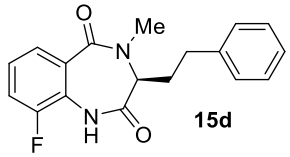

15d

This compound was obtained as36.3 mg of a white solid (116 µmol, 61%).

^{1}H-NMR (600 MHz, $CDCl_3$)**:** δ [ppm] = 8.20 (bs, 1 H), 7.81–7.69 (m, 1 H), 7.31–7.00 (m, 7 H)*, 4.08 (bs, 0.3 H), 3.95 (t, *J* = 7.4 Hz, 0.7 H), 3.25 (s, 0.9 H), 3.13 (s, 2.1 H), 2.75–2.58 (m, 2 H), 2.44–2.36 (m, 0.7 H), 2.24–2.15 (m, 0.7 H), 1.97 (bs, 0.3 H), 1.80 (bs, 0.3 H).

* Signal overlaps with solvent residual peak.

^{13}C{^{1}H}-NMR (151 MHz, $CDCl_3$)**:** δ [ppm] = 169.5, 167.7, 152.2 (d, *J* = 248 Hz), 140.3, 129.2, 128.7 (2C), 128.4 (2C), 126.7, 126.6, 125.6 (d, *J* = 7.3 Hz), 124.7 (d, *J* = 13.1 Hz), 118.3 (d, *J* = 19.7 Hz), 55.0, 32.5, 29.3, 28.3.

^{19}F{^{1}H}-NMR (282 MHz, $CDCl_3$)**:** δ [ppm] = –127.9 (s, 0.8 F), –128.3 (s, 0.2 F).

NMR spectra showed a mixture of conformers. Only the ^{13}C signals of the major conformer are given.

HR-MS (ESI+)**:** *m/z* calcd. for $C_{18}H_{17}FN_2O_2$ $[M+Na]^+$: 335.1166, found: 335.1165.

HPLC: t_R = 10.8 min.

Specific rotation: $[\alpha]_D$ = +55.3 °·mL·dm^{-1}·g^{-1} (ρ = 0.89; $CHCl_3$).

(*S*)-7-chloro-4-methyl-3-phenethyl-3,4-dihydro-1*H*-benzo[1,4]diazepine-2,5-dione (**15e**)

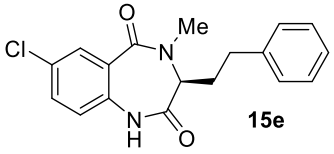

15e

This compound was obtained as 14.1 mg of a white solid (42.9 µmol, 23%).

^{1}H-NMR (600 MHz, $CDCl_3$)**:** δ [ppm] = 9.00 (bs, 0.3 H), 8.79 (bs, 0.7 H), 7.96 (d, *J* = 2.5 Hz, 0.3 H), 7.90 (d, *J* = 2.5 Hz, 0.7 H), 7.42 (dd, *J* = 8.5, 2.5 Hz, 1 H), 7.27–7.24 (m, 2 H)*, 7.21–7.12 (m, 2.5 H), 7.04 (d, *J* = 7.3 Hz, 0.5 H), 6.96 (d, *J* = 8.5 Hz, 0.7 H), 6.92 (d, *J* = 8.5 Hz, 0.3 H), 4.03 (bt, *J* = 7.4 Hz, 0.3 H), 3.94 (t, *J* = 7.4 Hz, 0.7 H), 3.24 (s, 0.9 H), 3.12 (s, 2.1 H), 2.73–2.57 (m ,2 H), 2.44–2.36 (m, 0.7 H), 2.23–2.15 (m, 0.7 H), 1.92 (bs, 0.3 H), 1.83 (bs, 0.3 H).

* Signal overlaps with solvent residual peak.

^{13}C{^{1}H}-NMR (151 MHz, $CDCl_3$)**:** δ [ppm] = 170.3, 167.5, 140.2, 134.1, 132.6, 131.2, 131.1, 128.9, 128.8 (2C), 128.4 (2C), 126.7, 122.1, 55.0, 32.6, 29.3, 28.3.

HR-MS (ESI+)**:** *m/z* calcd. for $C_{18}H_{17}ClN_2O_2$ $[M+Na]^+$: 351.0871, 353.0842; found: 351.0869, 353.0845.

HPLC: t_R = 12.0 min.

Specific rotation: $[\alpha]_D$ = +51.0 °·mL·dm^{-1}·g^{-1} (ρ = 0.71; $CHCl_3$).

(*S*)-8-chloro-4-methyl-3-phenethyl-3,4-dihydro-1*H*-benzo[1,4]diazepine-2,5-dione (**15f**)

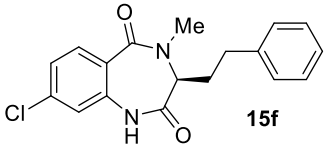

15f

This compound was obtained as 27.2 mg of a white solid (82.7 µmol, 44%).

^{1}H-NMR (600 MHz, $CDCl_3$)**:** δ [ppm] = 9.23 (bs, 0.3 H), 9.09 (bs, 0.7 H), 7.94 (d, *J* = 8.4 Hz, 0.3 H), 7.87 (d, *J* = 8.4 Hz), 7.27–7.21 (m, 3 H)*, 7.20–7.13 (m, 2.5 H), 7.06–6.99 (m, 1.5 H), 4.04 (t, *J* = 7.3 Hz, 0.3 H), 3.93 (t, *J* = 7.3 Hz, 0.7 H), 3.24 (s, 0.9 H), 3.12 (s, 2.1 H), 2.72–2.58 (m, 2 H), 2.44–2.36 (m, 0.7 H), 2.24–2.15 (m, 0.7 H), 1.96–1.88 (bs, 0.3 H), 1.86–1.81 (bs, 0.3 H).
* Signal overlaps with solvent residual peak.
^{13}C{^{1}H}-NMR (151 MHz, $CDCl_3$)**:** δ [ppm] = 170.5, 168.0, 140.3, 138.3, 136.7, 132.9, 128.8 (2C), 128.4 (2C), 126.6, 126.0, 125.7, 120.6, 55.0, 35.6, 29.3, 28.4.
NMR spectra showed a mixture of conformers. Only the ^{13}C signals of the major conformer are given.
HR-MS (ESI+)**:** *m/z* calcd. for $C_{18}H_{17}ClN_2O_2$ $[M+Na]^+$: 351.0871, 353.0842; found: 351.0875, 353.0848.
HPLC: t_R = 12.0 min.
Specific rotation: $[\alpha]_D$ = +20.8 °·mL·dm^{-1}·g^{-1} (ρ = 0.88; $CHCl_3$).

(*S*)-4,7-dimethyl-3-phenethyl-3,4-dihydro-1*H*-benzo[1,4]diazepine-2,5-dione (**15h**)

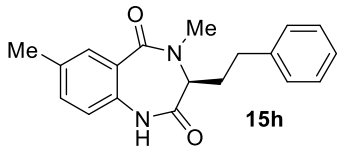

15h

This compound was obtained as 33.5 mg of a white solid (108 µmol, 57%).
^{1}H-NMR (600 MHz, $CDCl_3$)**:** δ [ppm] = 9.06 (bs, 0.3 H), 8.83 (bs, 0.7 H), 7.77 (bs, 0.3 H), 7.73 (bs, 0.7 H), 7.28–7.21 (m, 3 H)*, 7.19–7.13 (m, 2.4 H), 7.03 (bd, *J* = 8.5 Hz, 0.6 H), 6.92 (bd, *J* = 8.1 Hz, 0.7 H), 6.88 (bd, *J* = 8.1 Hz, 0.3 H), 4.03 (bt, *J* = 8.3 Hz, 0.3 H), 3.98 (bt, *J* = 7.3 Hz, 0.7 H), 3.25 (s, 0.9 H), 3.12 (s, 2.1 H), 2.64–2.54 (m, 2 H), 2.44–2.38 (m, 0.7 H), 2.37 (s, 3 H), 2.21–2.13 (m, 0.7 H), 1.94–1.86 (m, 0.3 H), 1.85–1.77 (m, 0.3 H).
* Signal overlaps with solvent residual peak.
^{13}C{^{1}H}-NMR (151 MHz, $CDCl_3$)**:** δ [ppm] = 170.5, 168.9, 140.6, 135.4, 133.3, 131.4, 128.7 (2C), 128.4 (2C), 127.4, 126.5, 126.5, 120.7, 55.1, 32.7, 29.2, 28.5, 20.8.
NMR spectra showed a mixture of conformers. Only the ^{13}C signals of the major conformer are given.
HR-MS (ESI+)**:** *m/z* calcd. for $C_{19}H_{20}N_2O_2$ $[M+Na]^+$: 331.1417, found: 331.1421.
HPLC: t_R = 11.8 min.
Specific rotation: $[\alpha]_D$ = +62.7 °·mL·dm^{-1}·g^{-1} (ρ = 1.15; $CHCl_3$).

(*S*)-4-methyl-3-phenethyl-3,4-dihydro-1*H*-naphtho[2,3-*e*][1,4]diazepine-2,5-dione (**15i**)

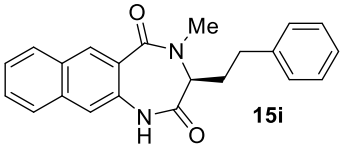

15i

This compound was obtained as 15.7 mg of a white solid (45.6 µmol, 24%).
^{1}H-NMR (600 MHz, $CDCl_3$)**:** δ [ppm] = 8.88 (bs, 0.3 H), 8.68 (bs, 0.7 H), 8.58 (s, 0.3 H), 8.51 (s, 0.7 H), 7.93 (dd, *J* = 8.4, 1.2 Hz, 1 H), 7.78 (bd, *J* = 8.2 Hz, 1 H), 7.57 (ddd, *J* = 8.1, 6.6, 1.2 Hz, 1 H), 7.53–7.48 (m, 1 H), 7.45 (bs, 0.7 H), 7.38 (bs, 0.3 H), 7.24–7.17 (m, 2.2 H), 7.16–7.11 (m, 2.2 H), 6.99 (bd, *J* = 7.5 Hz, 0.6 H), 4.12–4.06 (m, 1 H), 3.31 (s, 1 H), 3.19 (s, 2 H), 2.72–2.55 (m, 2 H), 2.47–2.39 (m, 0.7 H), 2.24–2.16 (m, 0.7 H), 1.94–1.87 (m, 0.3 H), 1.84–1.77 (m, 0.3 H).
^{13}C{^{1}H}-NMR (151 MHz, $CDCl_3$)**:** δ [ppm] = 172.3, 171.0, 169.0, 166.4, 140.4, 139.4, 135.1, 134.9, 133.3, 132.7, 132.3, 131.5, 130.7, 130.4, 129.2, 129.1, 128.9, 128.7 (2C), 128.4 (2C), 127.3, 127.1, 126.9, 126.6, 126.5, 118.1, 117.1, 66.2, 55.1, 39.8, 32.7, 32.3, 31.0, 29.3, 28.5.
NMR spectra showed a mixture of conformers.
Due to ^{13}C-signal overlapping in the aromatic region, it was not possible to unambiguously assign the major conformer. Therefore, all signals are given.
HR-MS (ESI+)**:** *m/z* calcd. for $C_{22}H_{20}N_2O_2$ $[M+Na]^+$: 367.1417, found: 367.1416.
HPLC: t_R = 12.8 min.
Specific rotation: $[\alpha]_D$ = +26.7 °·mL·dm^{-1}·g^{-1} (ρ = 0.53; $CHCl_3$).

(*S*)-4-methyl-8-nitro-3-phenethyl-3,4-dihydro-1*H*-benzo[1,4]diazepine-2,5-dione (**15g**)

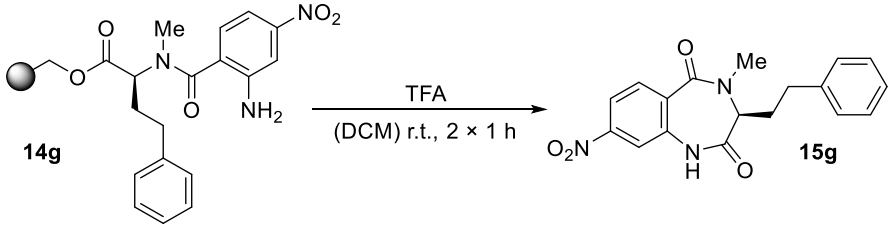

For the nitro compound, acid-induced cyclisation was used to obtain the cyclic final product due to base-sensitivity of the nitro group.

The resin was treated with 35% TFA in DCM for 1 hour, filtered, washed with DCM and the procedure was repeated one time. Combined filtrates were concentrated under reduced pressure and the residue was subjected to preparative HPLC to yield the product as 7.7 mg of a yellow solid (22.7 µmol, 12%).

^{1}H-NMR (600 MHz, $CDCl_3$)**:** δ [ppm] = 8.93 (bs, 0.3 H), 8.92 (bs, 0.7 H), 8.20–8.03 (m, 1.9 H), 7.32 (t, *J* = 7.5 Hz, 0.1 H), 7.26–7.23 (m, 2.1 H)*, 7.21–7.12 (m, 2.5 H), 7.02 (bs, 0.4 H), 4.11 (bs, 0.3 H), 3.90 (t, *J* = 7.5 Hz, 0.7 H), 3.28 (s, 0.9 H), 3.16 (s, 2.1 H), 2.73–2.60 (m, 2 H), 2.46–2.40 (m, 0.7 H), 2.28–2.20 (m, 0.7 H), 1.91 (bs, 0.3 H), 1.81 (bs, 0.3 H).

* Signal overlaps with solvent residual peak.

^{13}C{^{1}H}-NMR (151 MHz, $CDCl_3$)**:** δ [ppm] = 170.0, 167.0, 150.0, 139.9, 136.5, 133.3, 129.0, 128.9 (2C), 128.4 (2C), 126.8, 119.7, 116.0, 54.8, 32.5, 29.4, 28.2.

NMR spectra showed a mixture of conformers. Only the ^{13}C signals of the major conformer are given.

HR-MS (ESI+)**:** *m/z* calcd. for $C_{18}H_{17}N_3O_4$ $[M+Na]^+$: 340.1292, found: 340.1288.

HPLC: t_R = 11.9 min.

Specific rotation: $[\alpha]_D$ = +22.3 °·mL·dm^{-1}·g^{-1} (ρ = 0.47; $CHCl_3$).

4. NMR Spectra

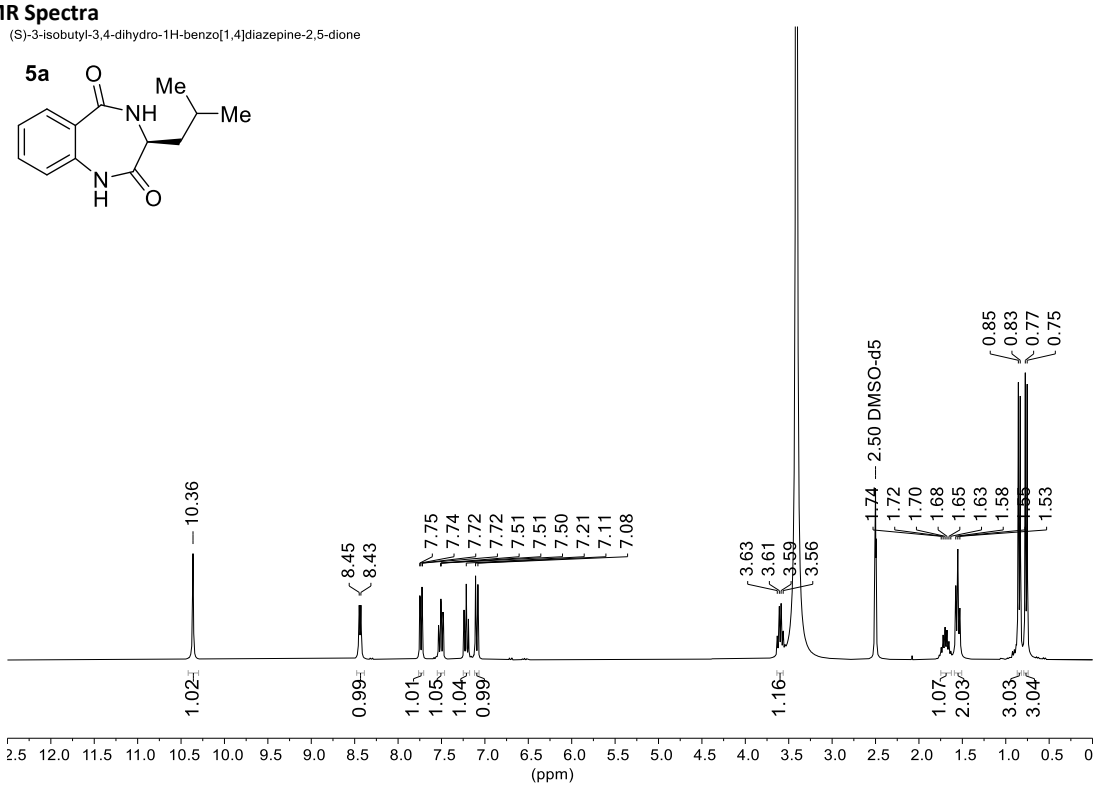

Figure S5. ^{1}H-NMR spectrum (400 MHz) of (*S*)-3-isobutyl-3,4-dihydro-1*H*-benzo[1,4]diazepine-2,5-dione (**5a**).

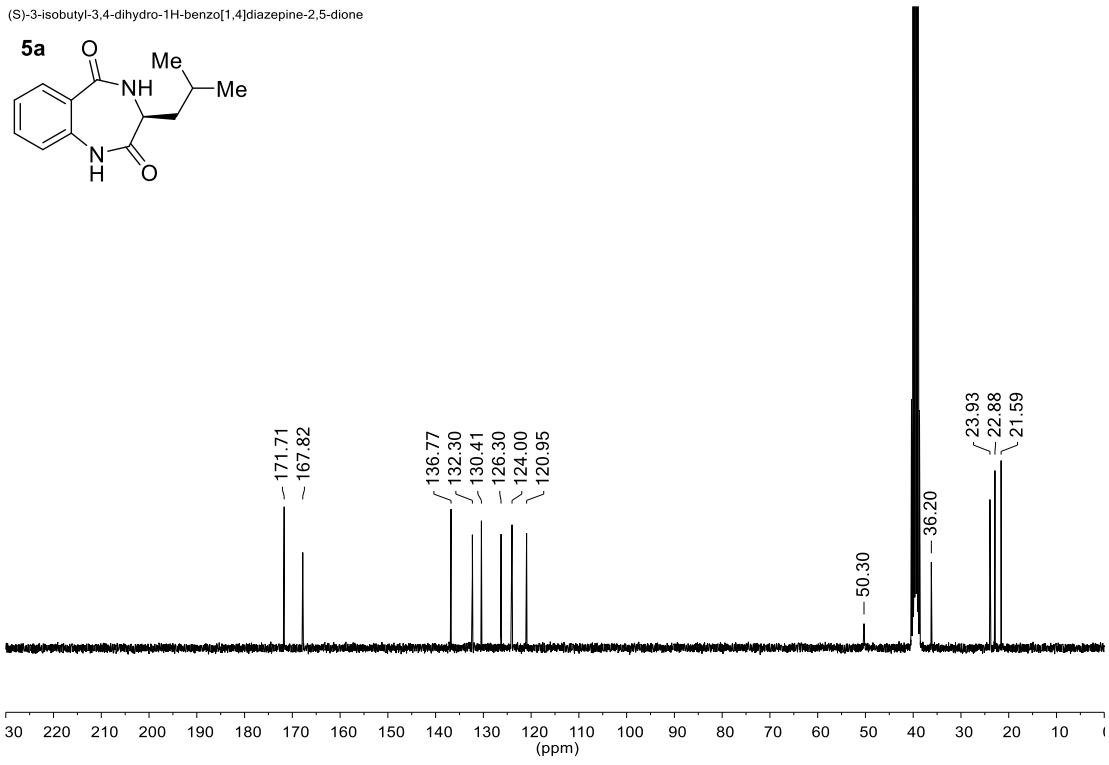

Figure S6. ^{13}C{^{1}H}-NMR spectrum (100 MHz) of (*S*)-3-isobutyl-3,4-dihydro-1*H*-benzo[1,4]diazepine-2,5-dione (**5a**).

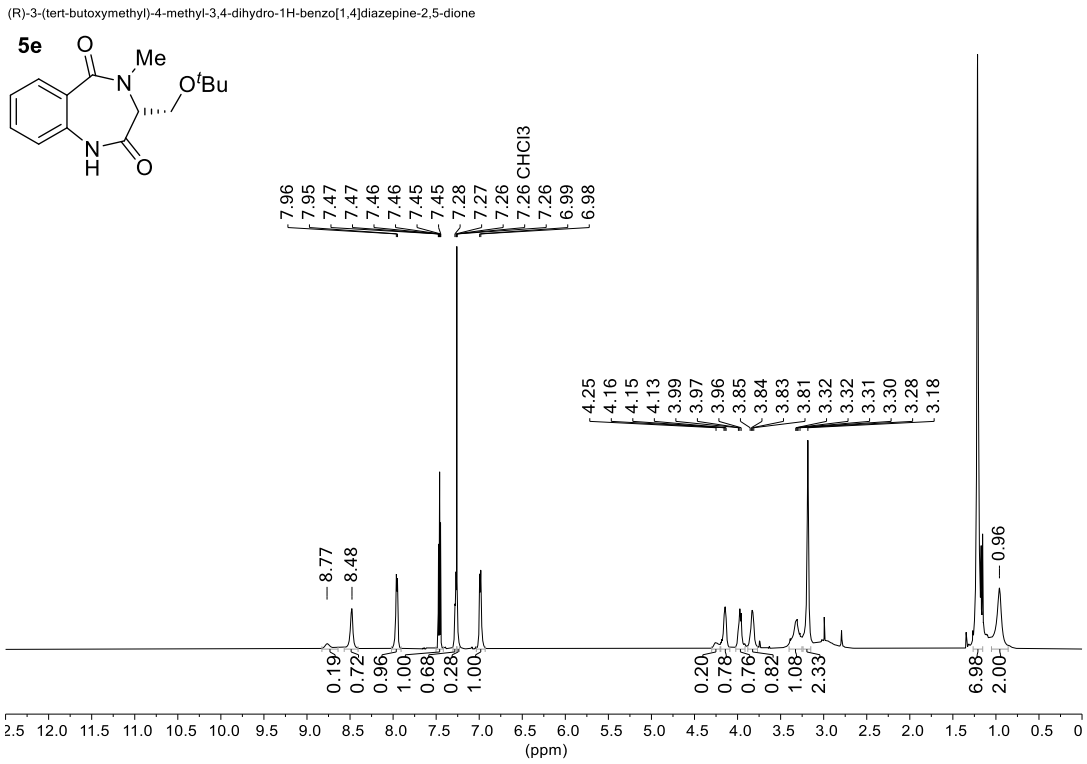

Figure S7. ^{1}H-NMR spectrum (600 MHz) of (*R*)-3-(*tert*-butoxymethyl)-4-methyl-3,4-dihydro-1*H*-benzo[1,4]diazepine-2,5-dione (**5e**).

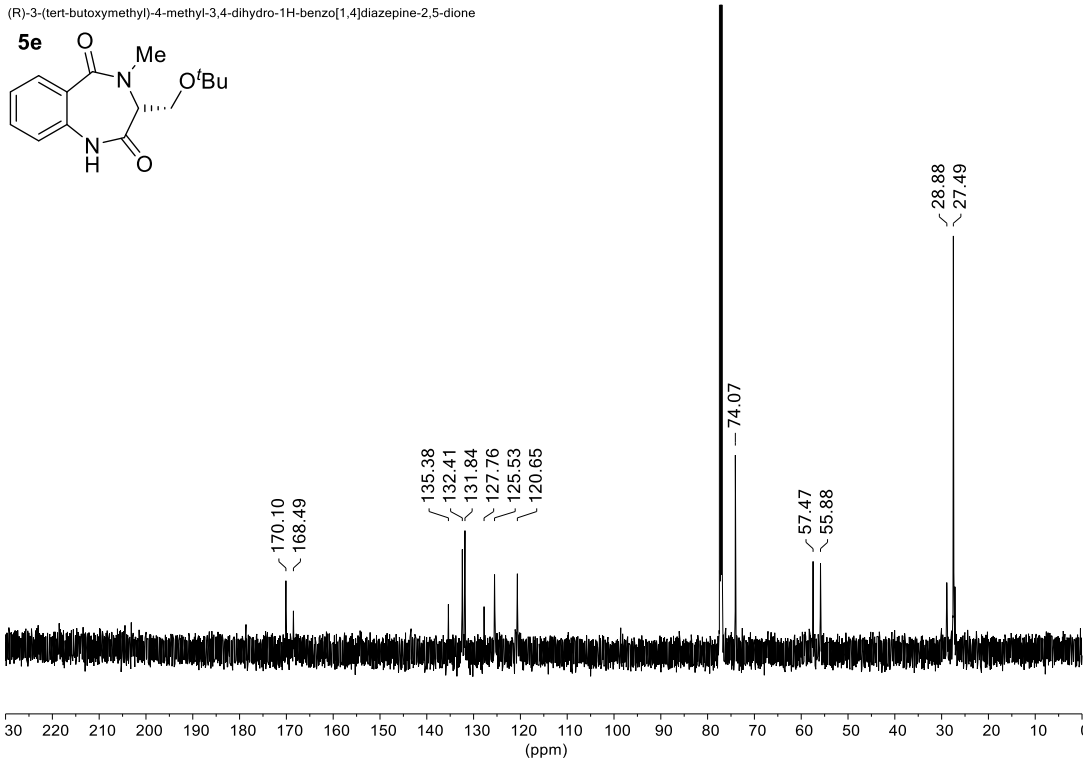

Figure S8. ^{13}C{^{1}H}-NMR spectrum (151 MHz) of (*R*)-3-(*tert*-butoxymethyl)-4-methyl-3,4-dihydro-1*H*-benzo[1,4]diazepine-2,5-dione (**5e**).

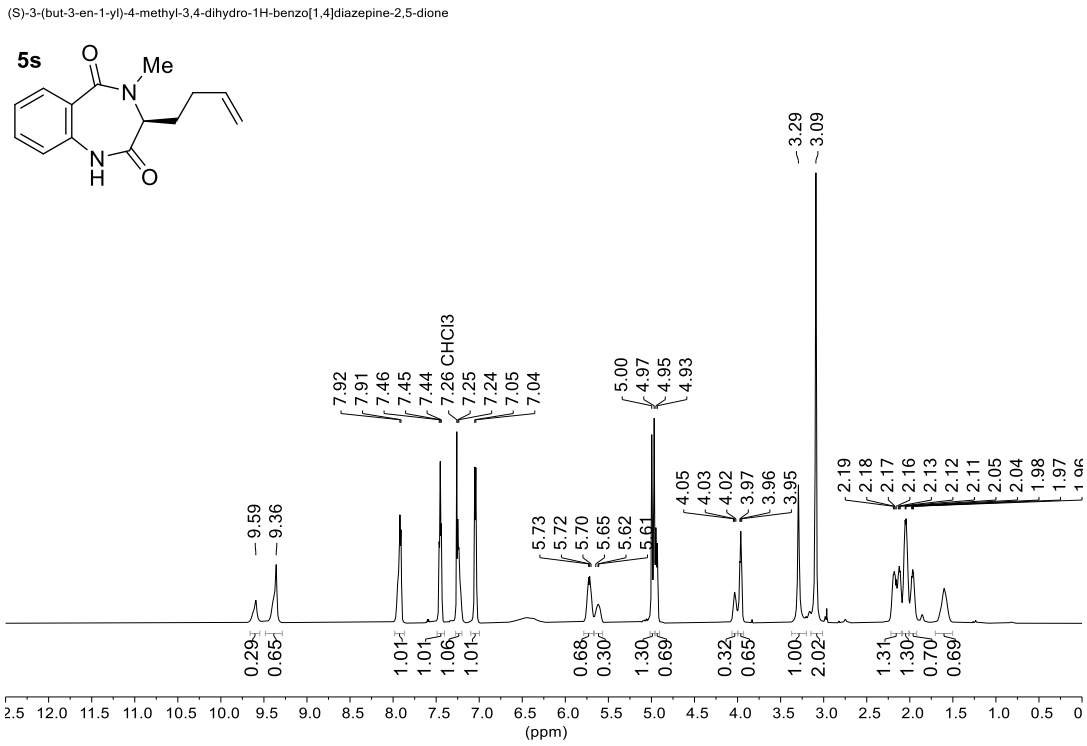

Figure S9. ^{1}H-NMR spectrum (600 MHz) of (*S*)-3-(but-3-en-1-yl)-4-methyl-3,4-dihydro-1*H*-benzo[1,4]diazepine-2,5-dione (**5s**).

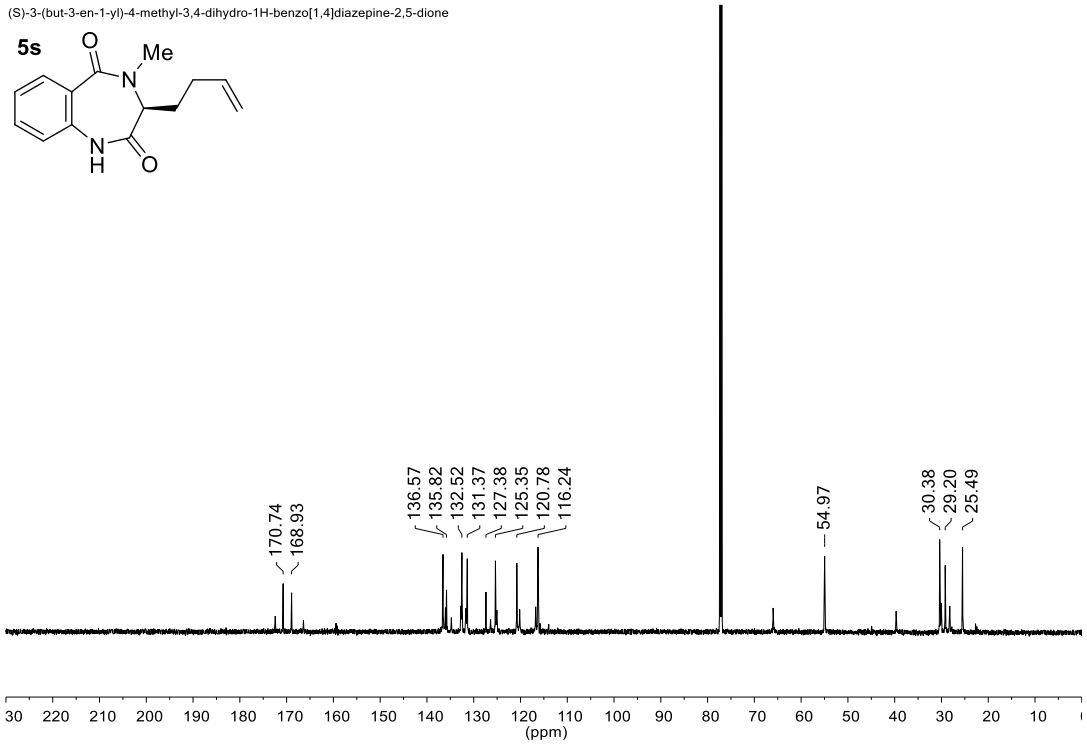

Figure S10. ^{13}C{^{1}H}-NMR spectrum (151 MHz) of (*S*)-3-(but-3-en-1-yl)-4-methyl-3,4-dihydro-1*H*-benzo[1,4]diazepine-2,5-dione (**5s**).

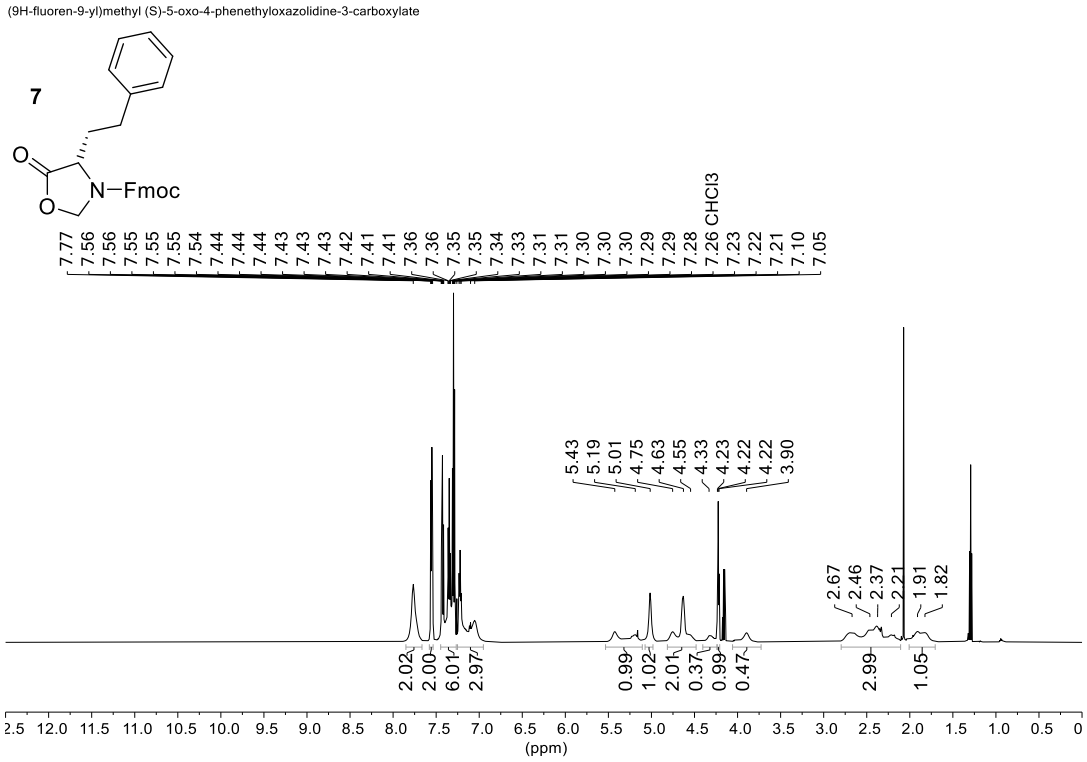

Figure S11. ^{1}H-NMR spectrum (600 MHz) of (9*H*-fluoren-9-yl)methyl (*S*)-5-oxo-4-phenethyloxazolidine-3-carboxylate (**7**).

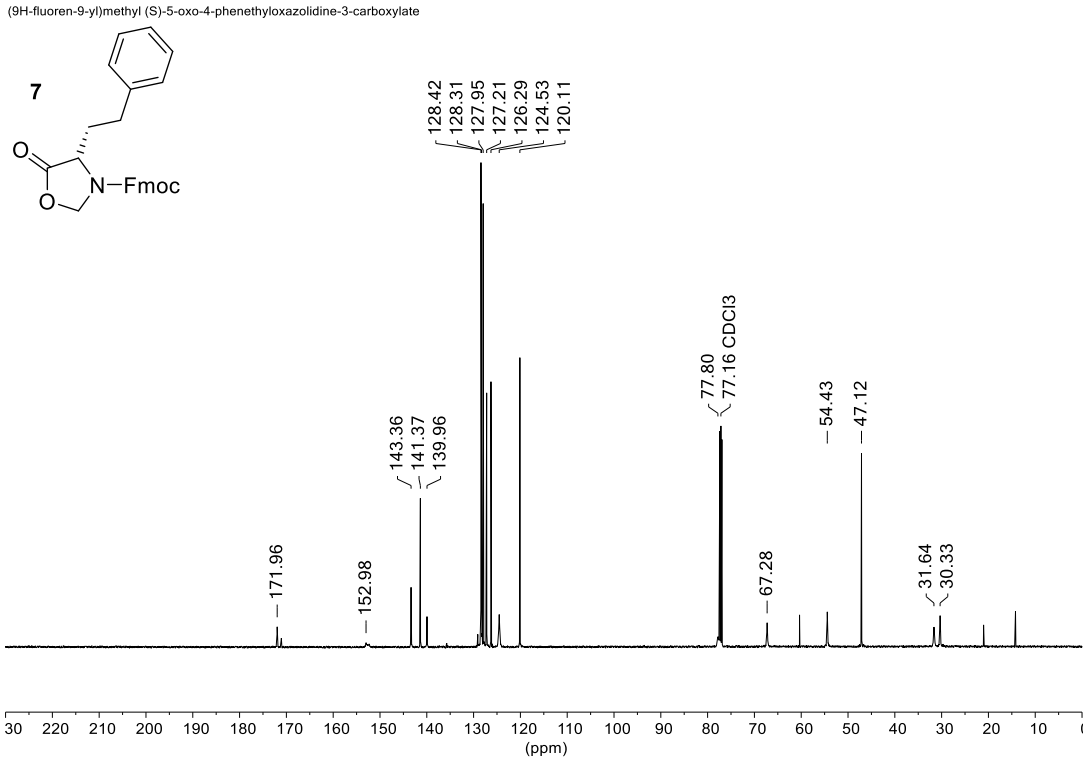

Figure S12. ^{13}C{^{1}H}-NMR spectrum (151 MHz) of (9*H*-fluoren-9-yl)methyl (*S*)-5-oxo-4-phenethyloxazolidine-3-carboxylate (**7**).

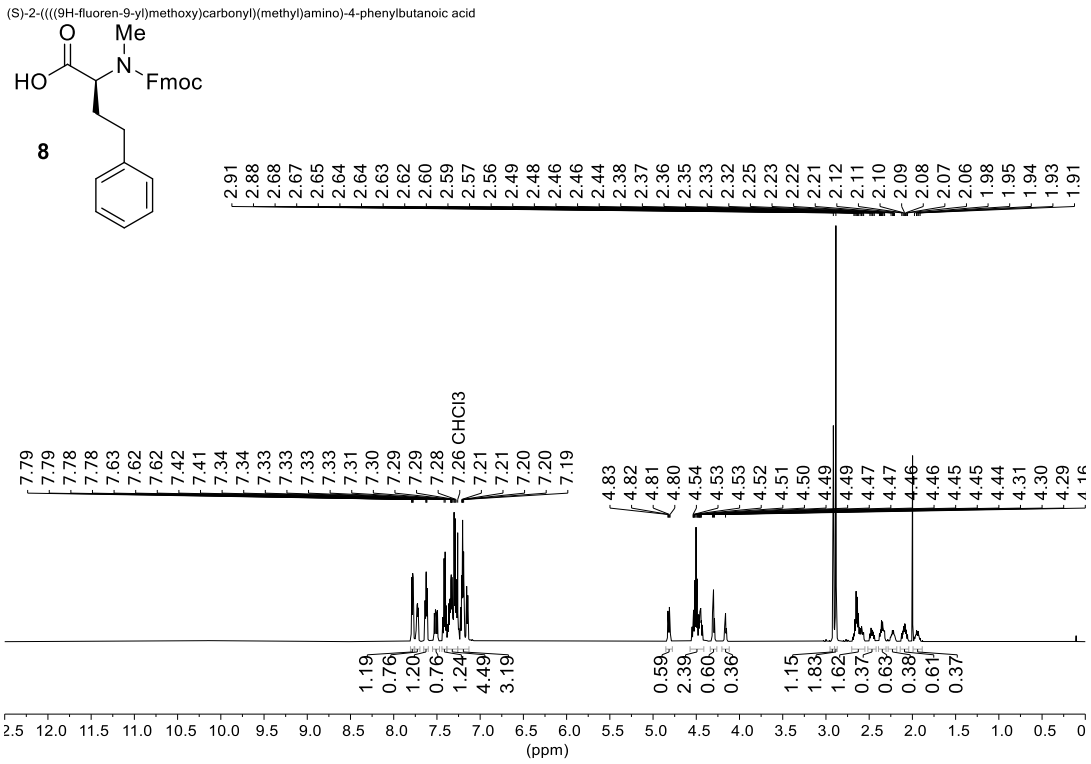

Figure S13. ^{1}H-NMR spectrum (600 MHz) of (*S*)-2-((((9*H*-fluoren-9-yl)methoxy)carbonyl)(methyl)amino)-4-phenylbutanoic acid (**8**).

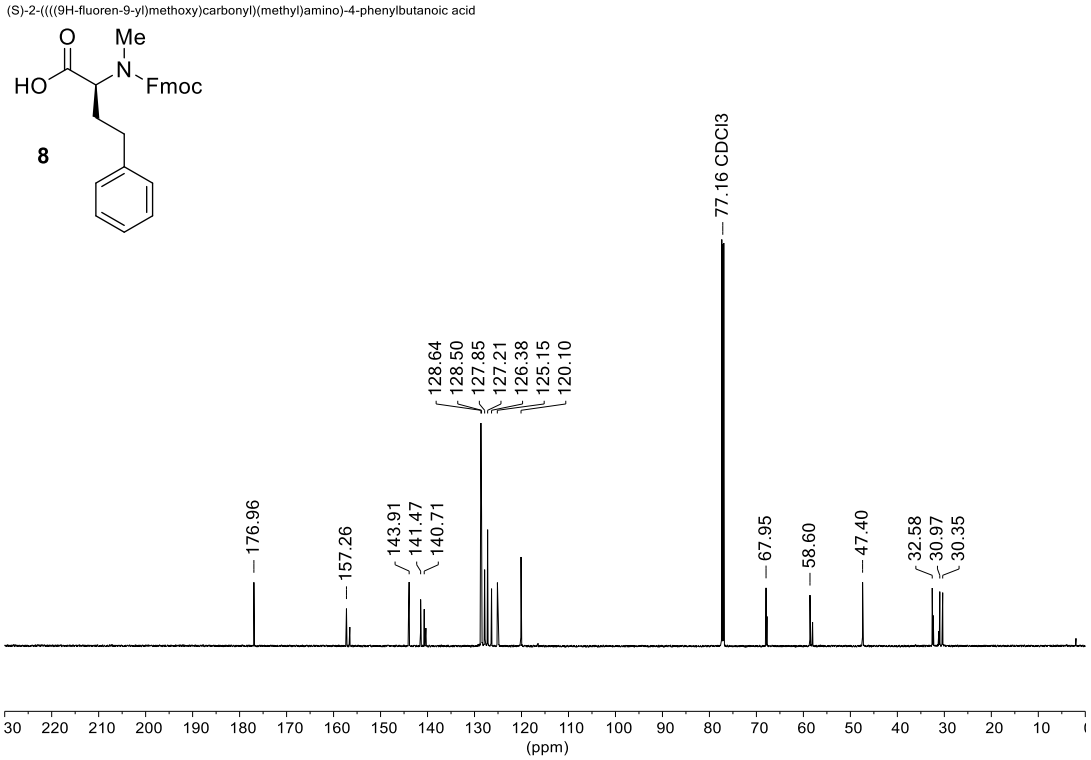

Figure S14. ^{13}C{^{1}H}-NMR spectrum (151 MHz) of (*S*)-2-((((9*H*-fluoren-9-yl)methoxy)carbonyl)(methyl)amino)-4-phenylbutanoic acid (**8**).

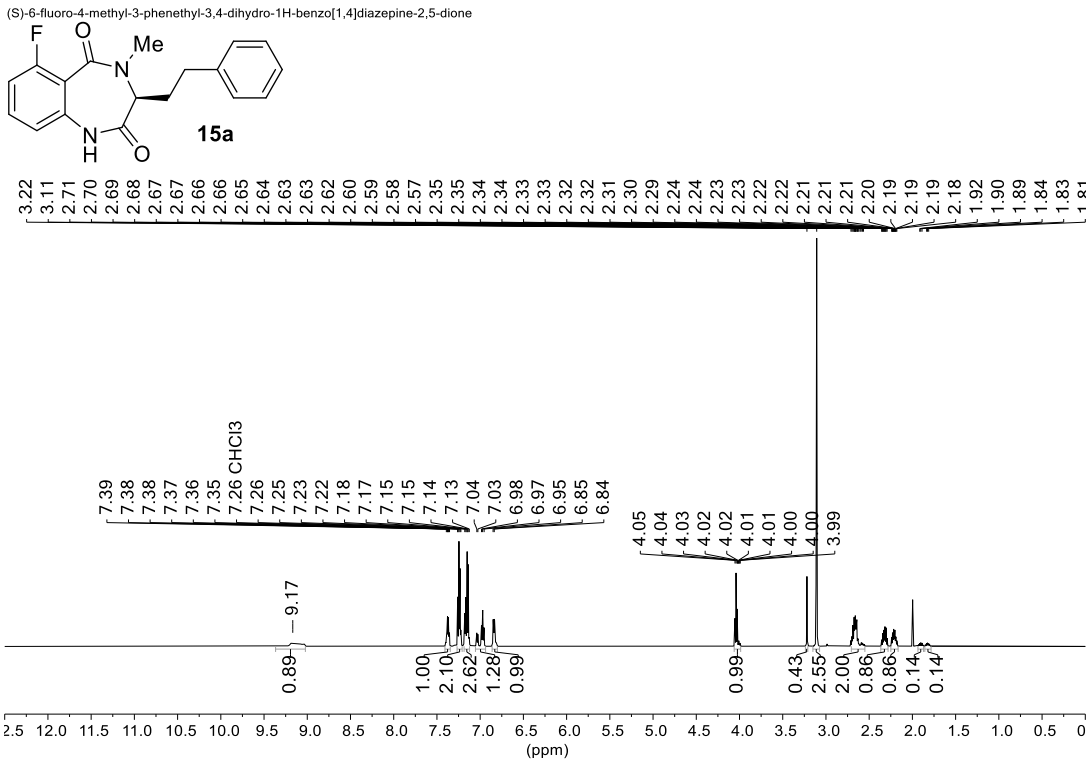

Figure S15. ^{1}H-NMR spectrum (600 MHz) of (*S*)-6-fluoro-4-methyl-3-phenethyl-3,4-dihydro-1*H*-benzo[1,4]diazepine-2,5-dione (**15a**).

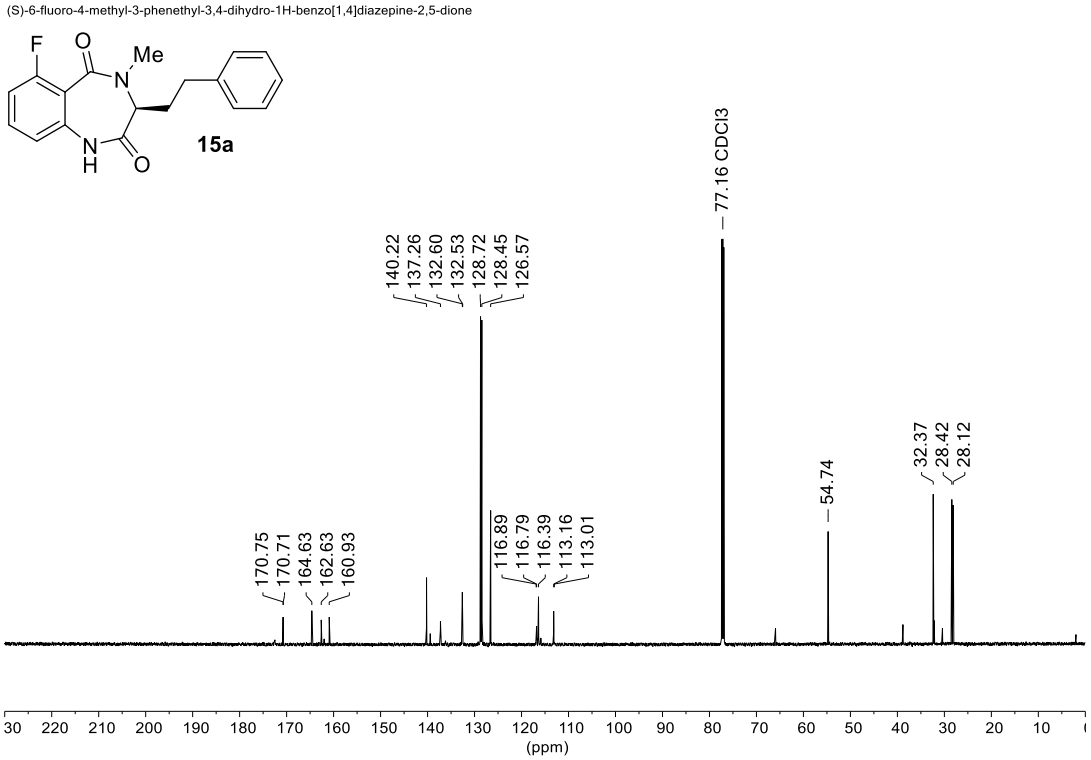

Figure S16. ^{13}C{^{1}H}-NMR spectrum (151 MHz) of (*S*)-6-fluoro-4-methyl-3-phenethyl-3,4-dihydro-1*H*-benzo[1,4]diazepine-2,5-dione (**15a**).

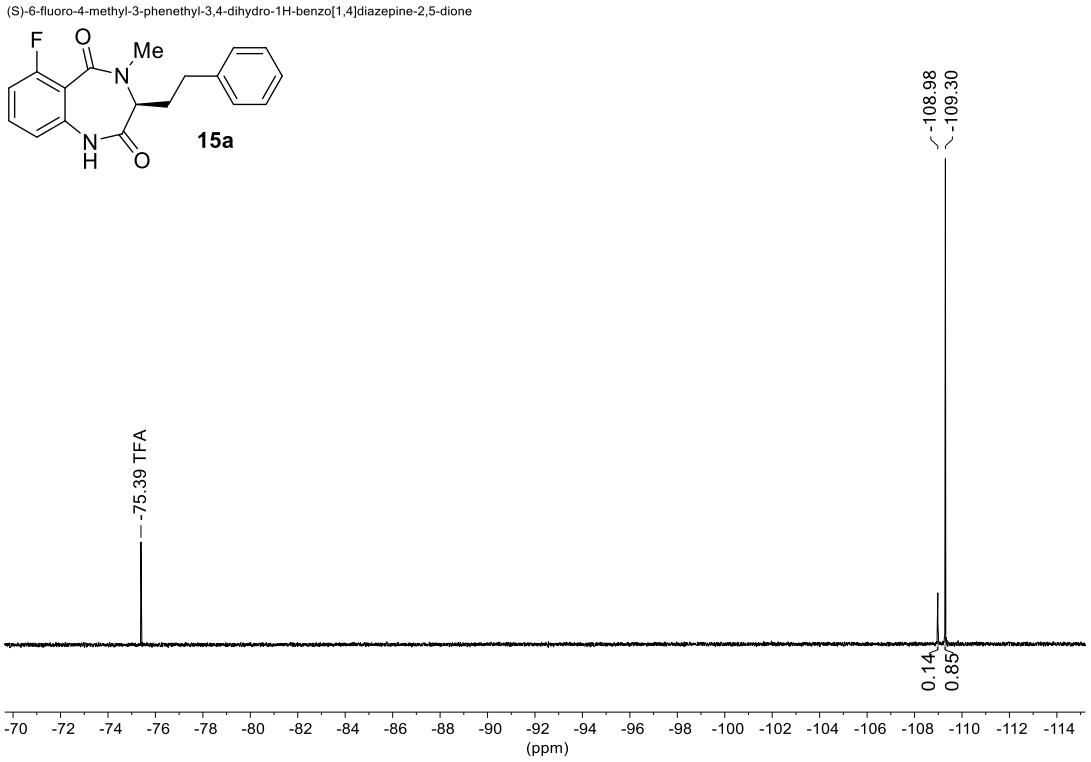

Figure S17. $^{19}F\{^{1}H\}$-NMR spectrum (282 MHz) of (*S*)-6-fluoro-4-methyl-3-phenethyl-3,4-dihydro-1*H*-benzo[1,4]diazepine-2,5-dione (**15a**).

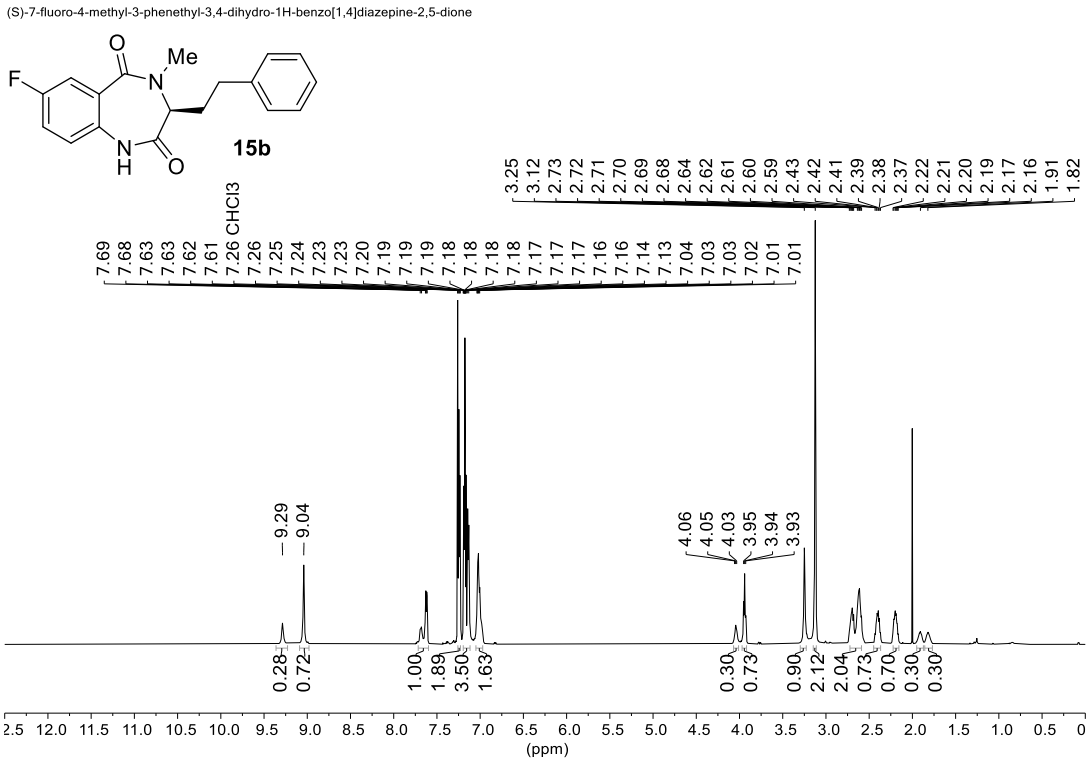

Figure S18. ^{1}H-NMR spectrum (600 MHz) of (*S*)-7-fluoro-4-methyl-3-phenethyl-3,4-dihydro-1*H*-benzo[1,4]diazepine-2,5-dione (**15b**).

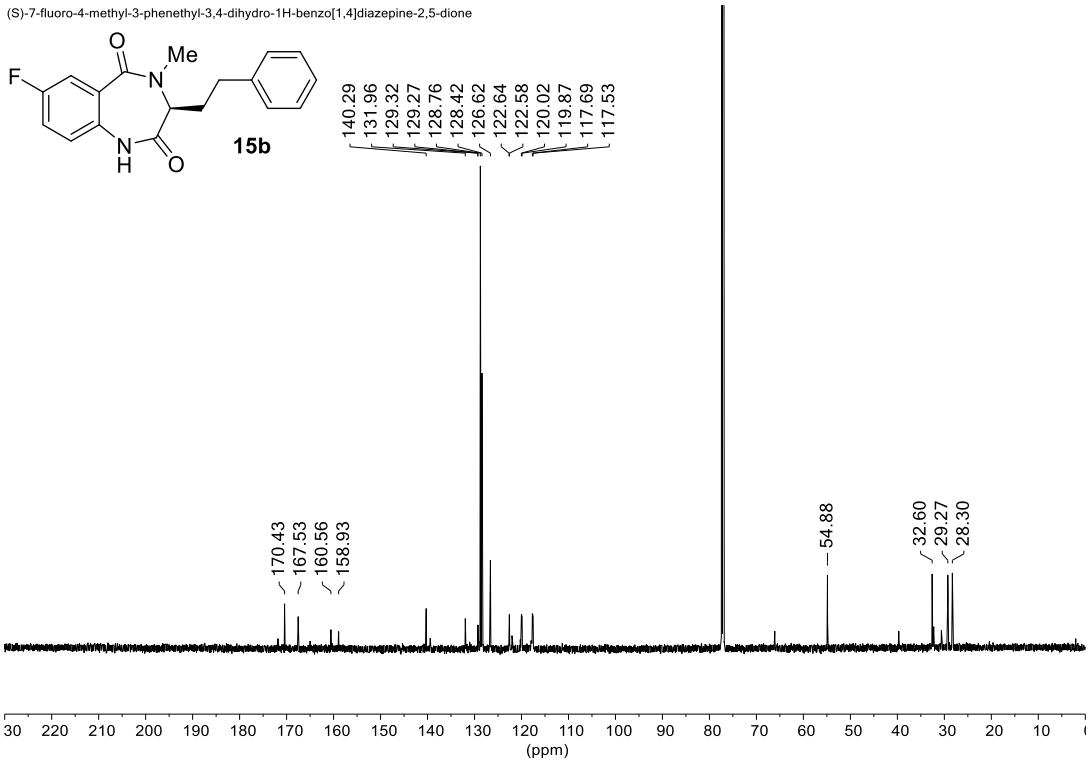

Figure S19. $^{13}C\{^{1}H\}$-NMR spectrum (151 MHz) of (*S*)-7-fluoro-4-methyl-3-phenethyl-3,4-dihydro-1*H*-benzo[1,4]diazepine-2,5-dione (**15b**).

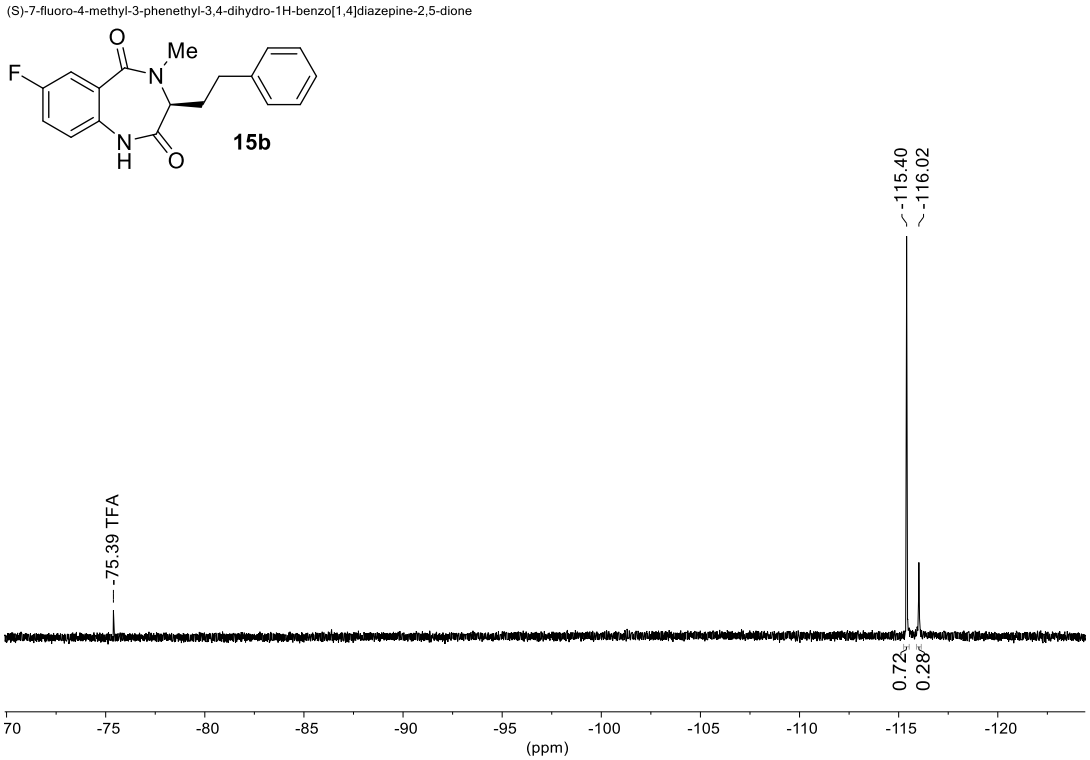

Figure S20. $^{19}F\{^{1}H\}$-NMR spectrum (282 MHz) of (*S*)-7-fluoro-4-methyl-3-phenethyl-3,4-dihydro-1*H*-benzo[1,4]diazepine-2,5-dione (**15b**).

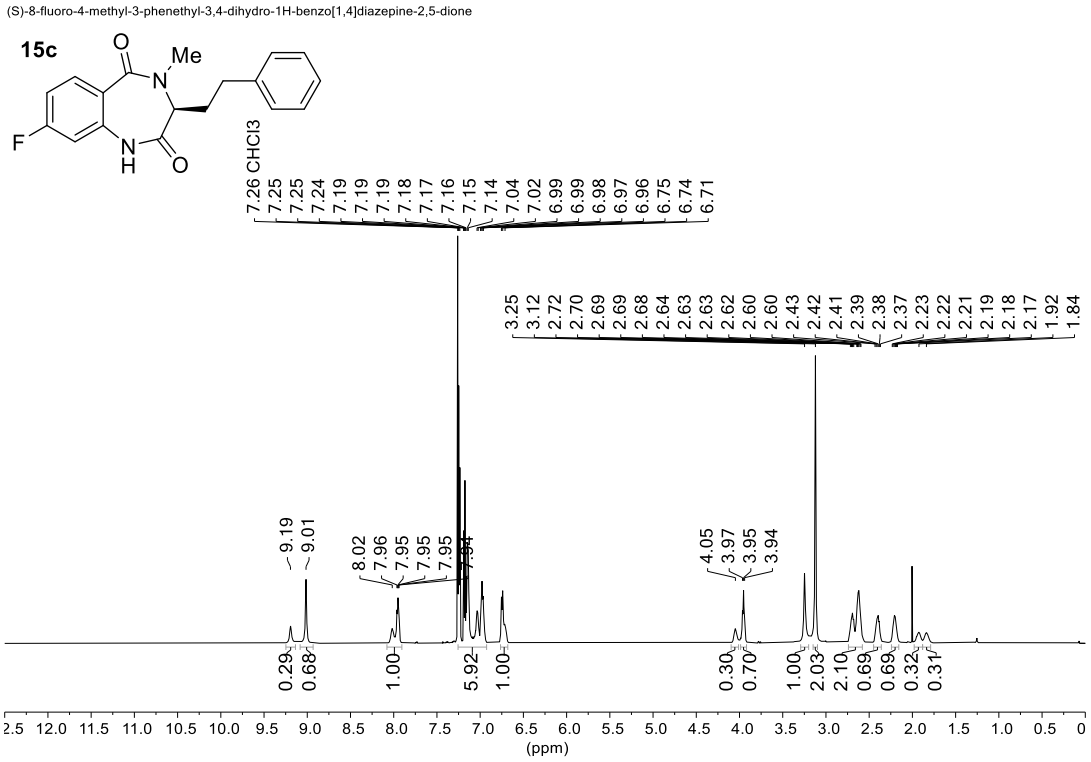

Figure S21. ^{1}H-NMR spectrum (600 MHz) of (*S*)-8-fluoro-4-methyl-3-phenethyl-3,4-dihydro-1*H*-benzo[1,4]diazepine-2,5-dione (**15c**).

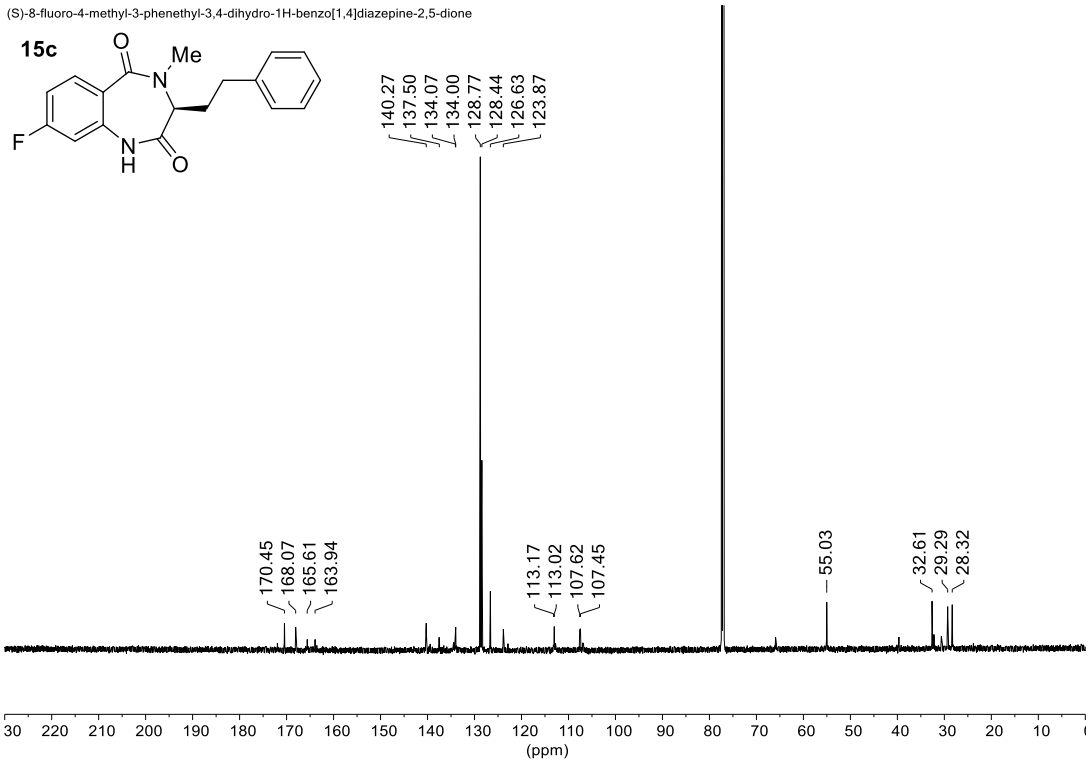

Figure S22. ^{13}C{^{1}H}-NMR spectrum (151 MHz) of (*S*)-8-fluoro-4-methyl-3-phenethyl-3,4-dihydro-1*H*-benzo[1,4]diazepine-2,5-dione (**15c**).

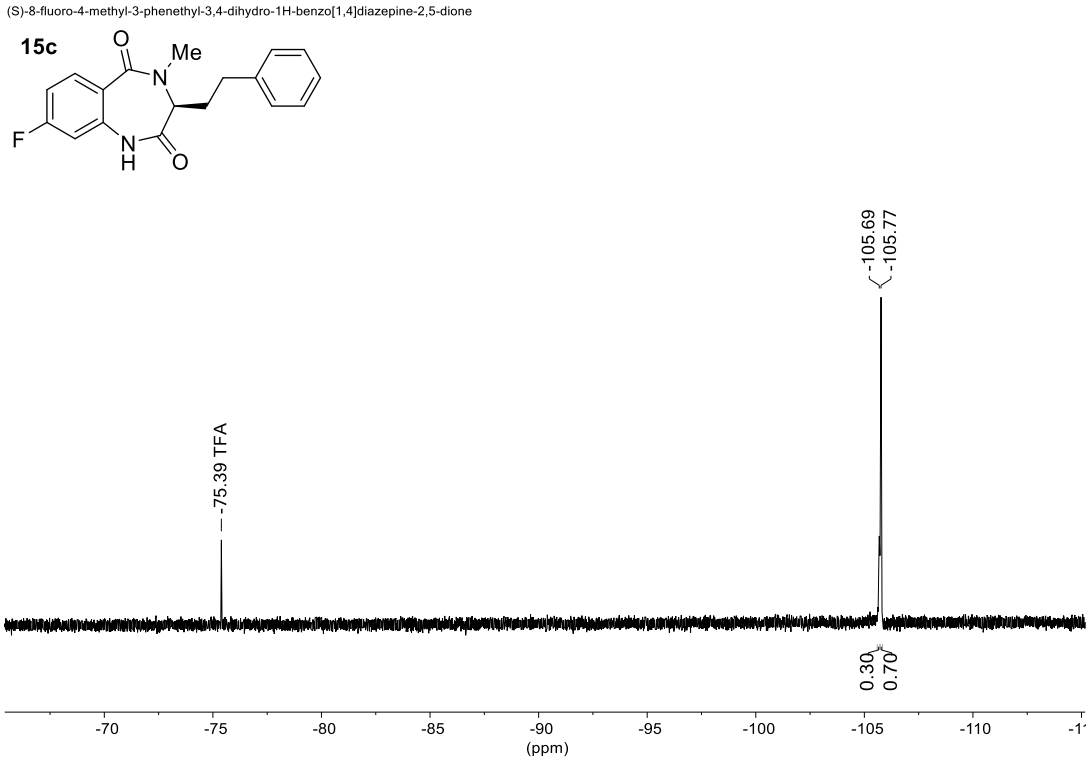

Figure S23. $^{19}F\{^{1}H\}$-NMR spectrum (282 MHz) of (*S*)-8-fluoro-4-methyl-3-phenethyl-3,4-dihydro-1*H*-benzo[1,4]diazepine-2,5-dione (**15c**).

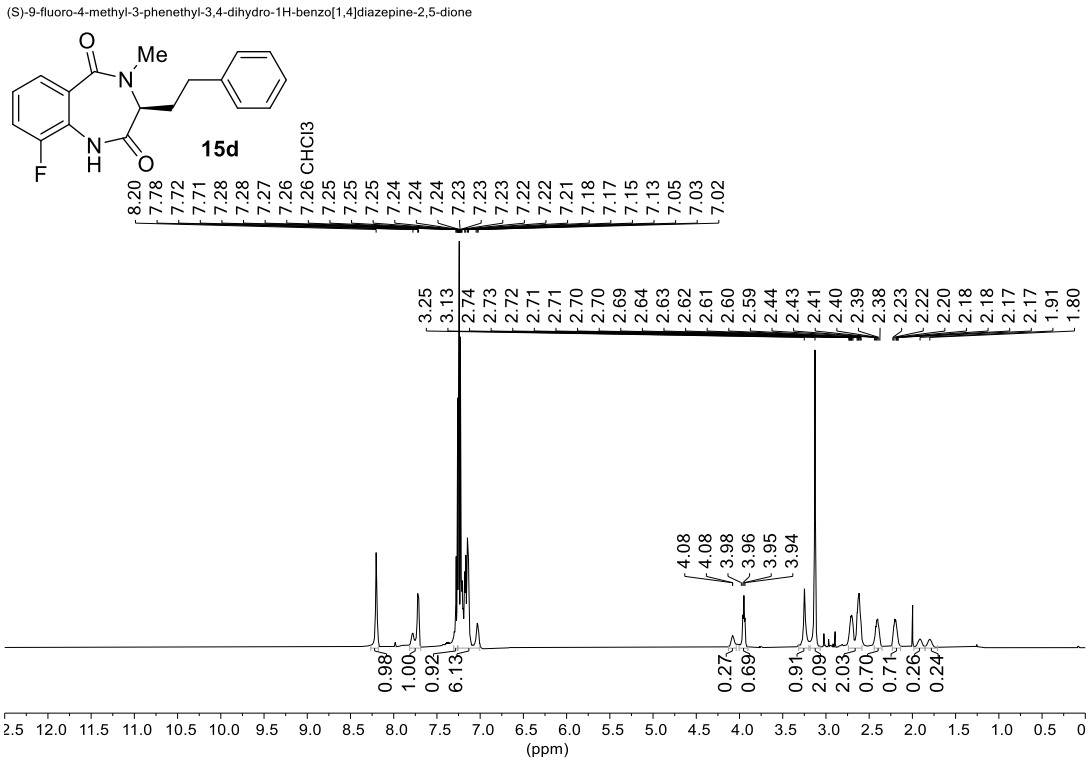

Figure S24. ^{1}H-NMR spectrum (600 MHz) of (*S*)-9-fluoro-4-methyl-3-phenethyl-3,4-dihydro-1*H*-benzo[1,4]diazepine-2,5-dione (**15d**).

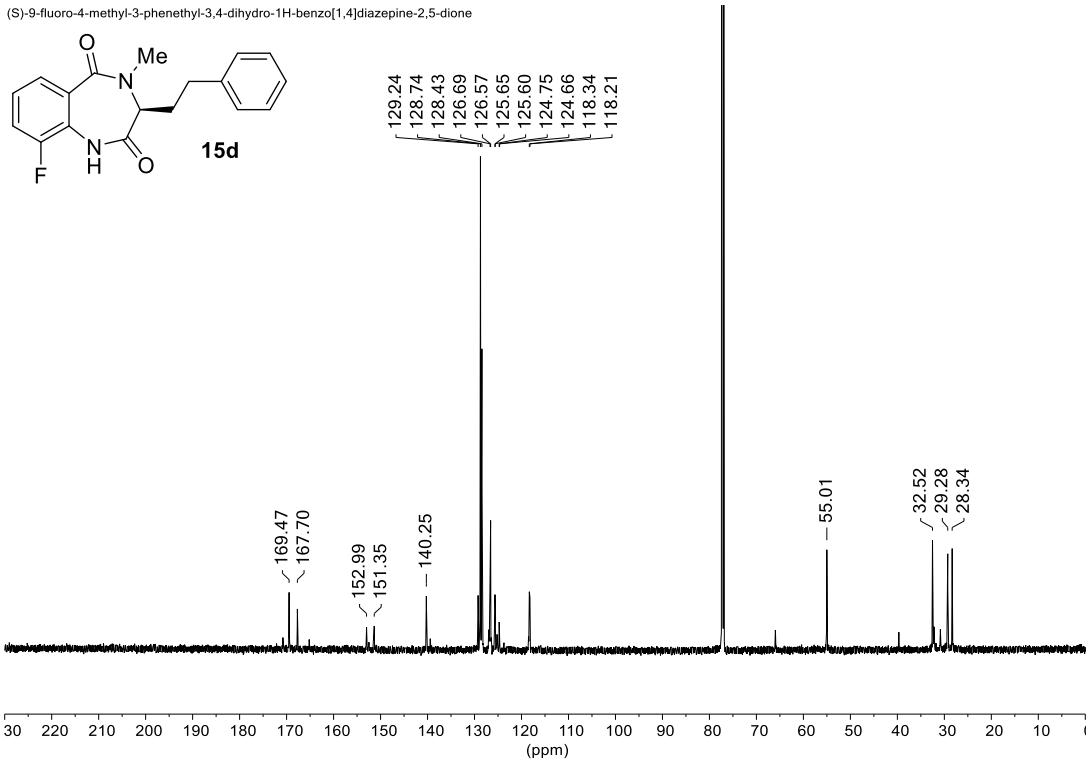

Figure S25. $^{13}C\{^{1}H\}$-NMR spectrum (151 MHz) of (*S*)-9-fluoro-4-methyl-3-phenethyl-3,4-dihydro-1*H*-benzo[1,4]diazepine-2,5-dione (**15d**).

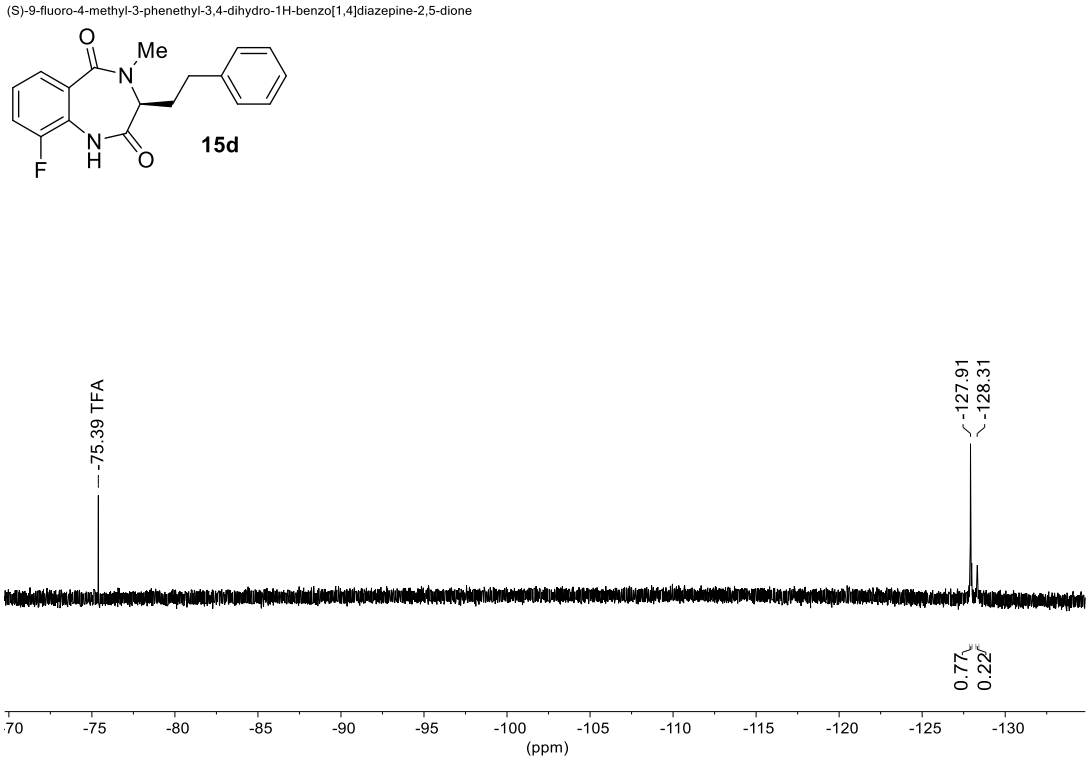

Figure S26. $^{19}F\{^{1}H\}$-NMR spectrum (282 MHz) of (*S*)-9-fluoro-4-methyl-3-phenethyl-3,4-dihydro-1*H*-benzo[1,4]diazepine-2,5-dione (**15d**).

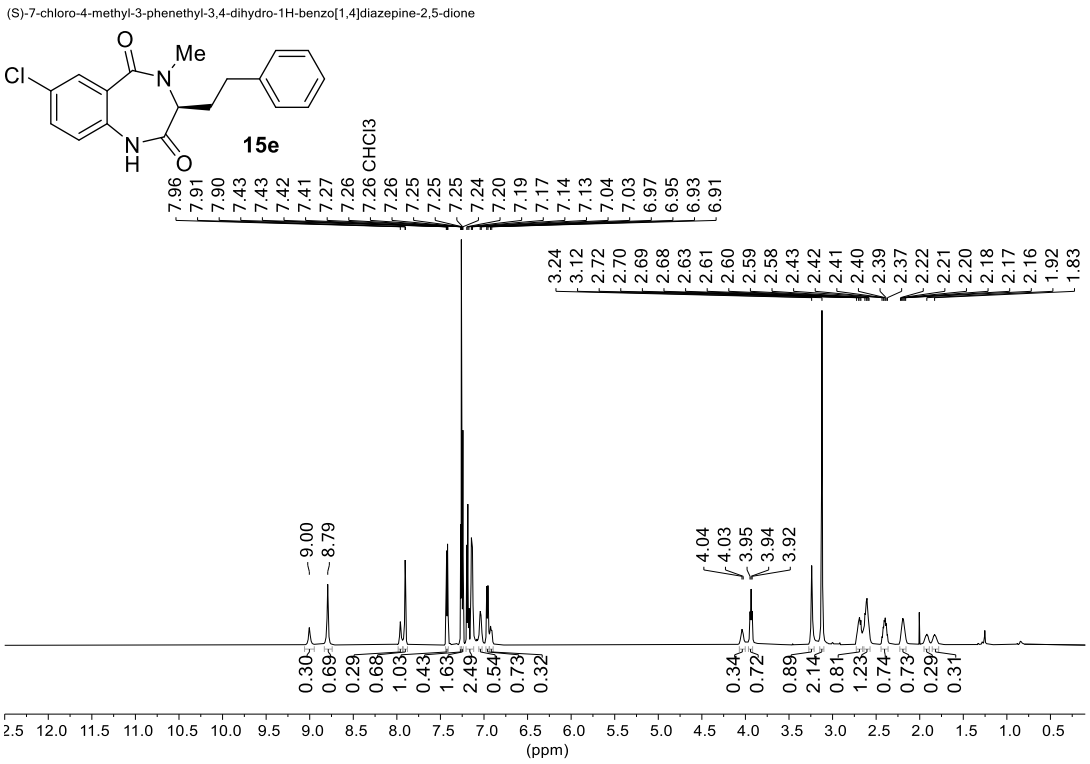

Figure S27. ^{1}H-NMR spectrum (600 MHz) of (*S*)-7-chloro-4-methyl-3-phenethyl-3,4-dihydro-1*H*-benzo[1,4]diazepine-2,5-dione (**15e**).

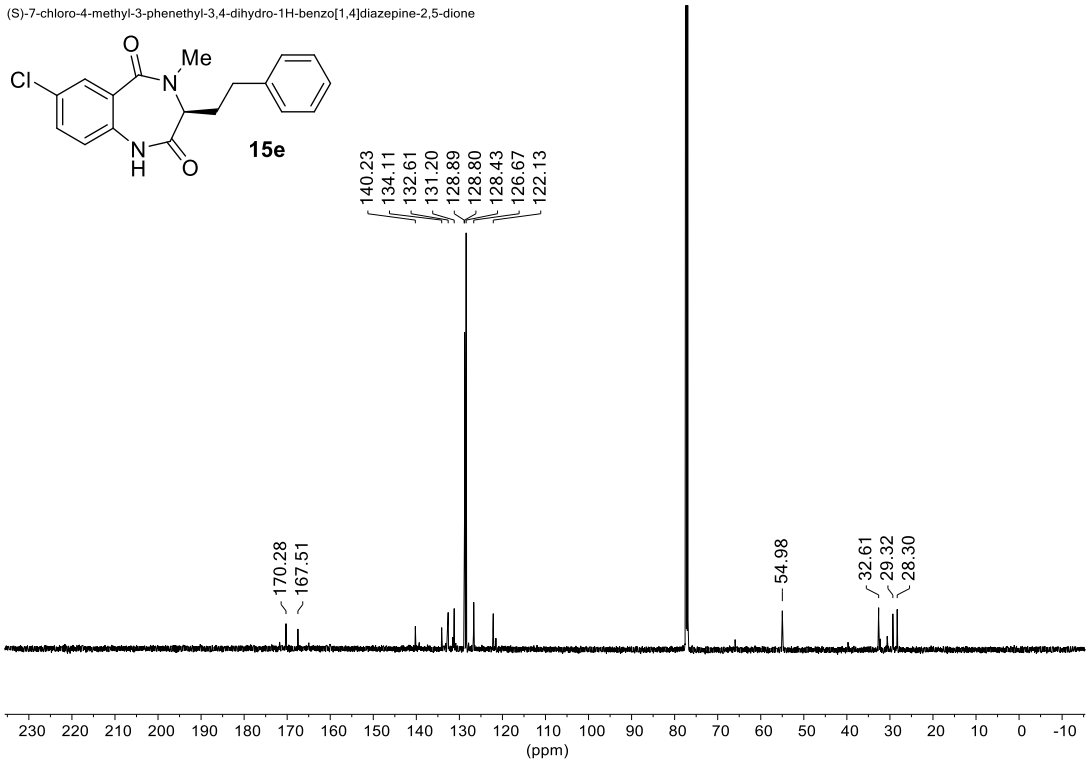

Figure S28. ^{13}C{^{1}H}-NMR spectrum (151 MHz) of (*S*)-7-chloro-4-methyl-3-phenethyl-3,4-dihydro-1*H*-benzo[1,4]diazepine-2,5-dione (**15e**).

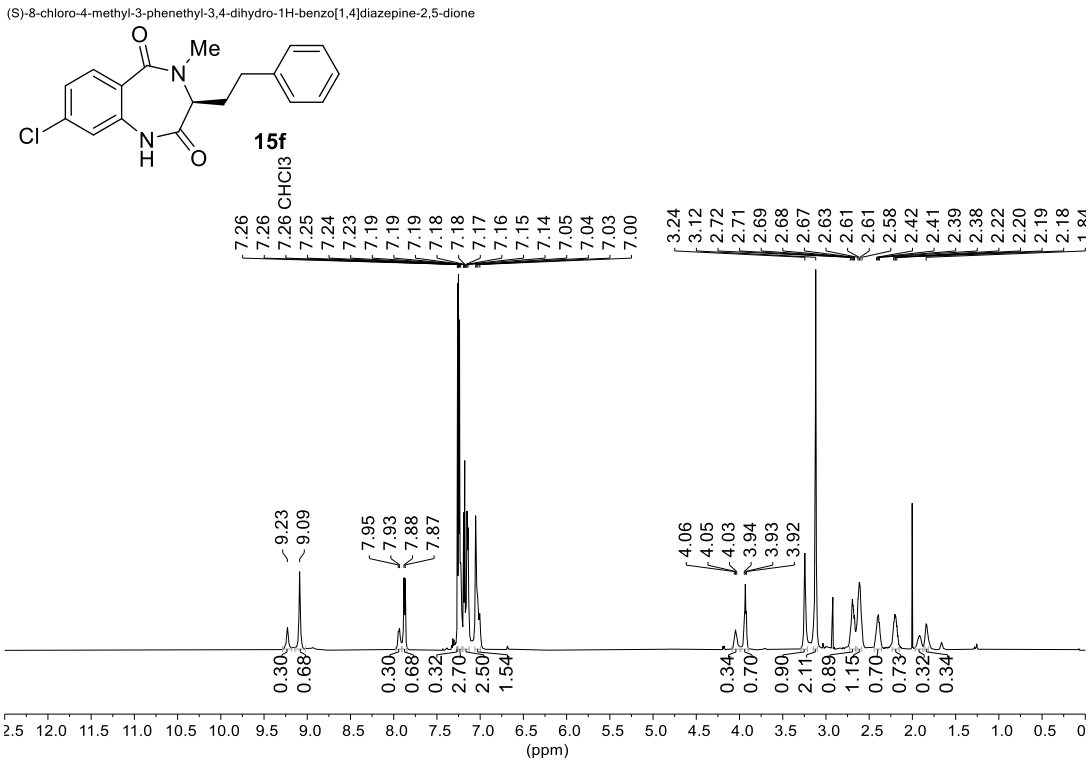

Figure S29. ^{1}H-NMR spectrum (600 MHz) of (*S*)-8-chloro-4-methyl-3-phenethyl-3,4-dihydro-1*H*-benzo[1,4]diazepine-2,5-dione (**15f**).

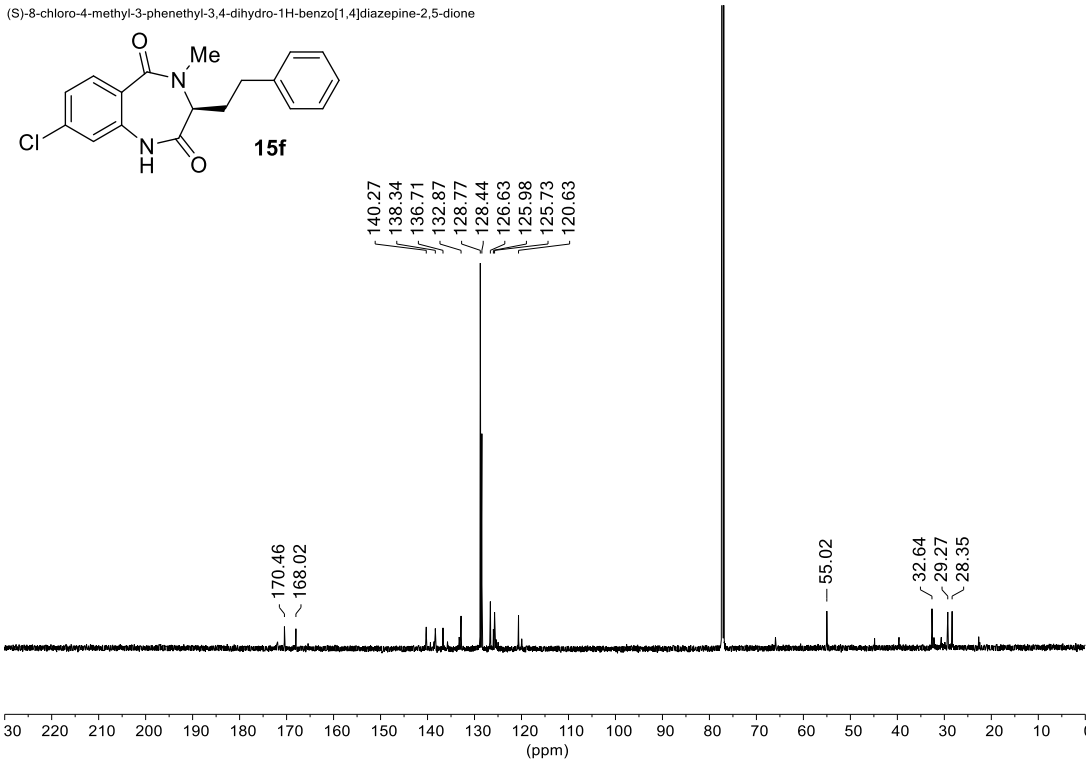

Figure S30. ^{13}C{^{1}H}-NMR spectrum of (*S*)-8-chloro-4-methyl-3-phenethyl-3,4-dihydro-1*H*-benzo[1,4]diazepine-2,5-dione (**15f**).

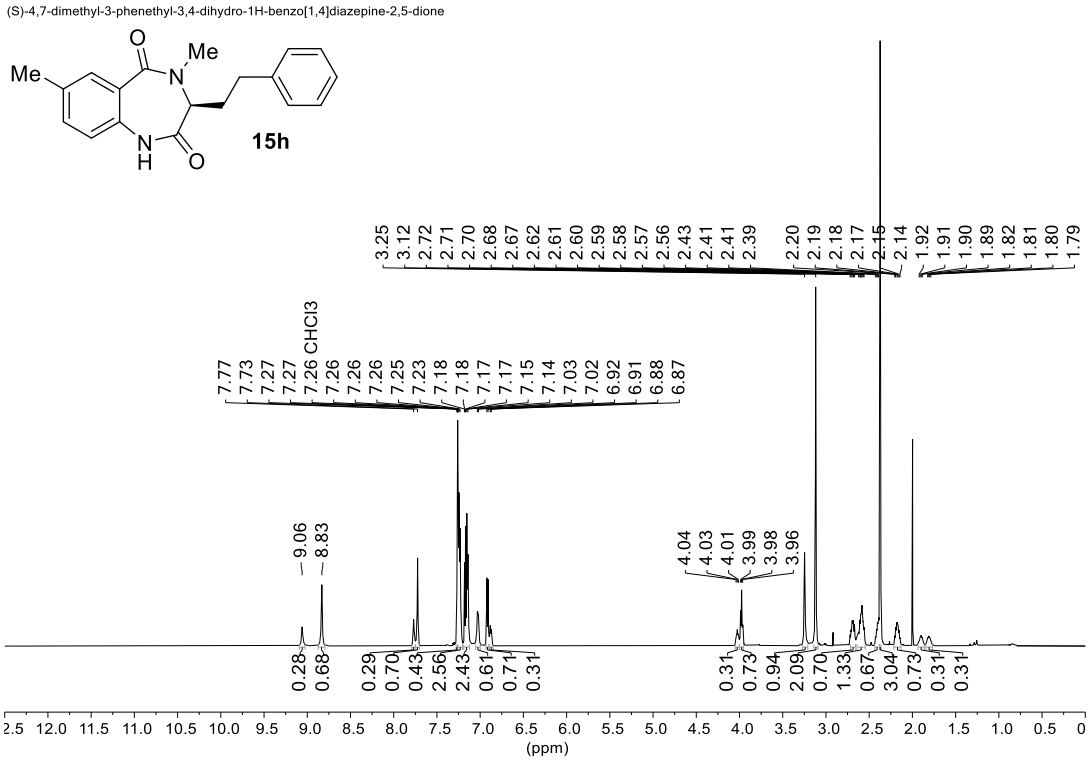

Figure S31. ^{1}H-NMR spectrum (600 MHz) of (*S*)-4,7-dimethyl-3-phenethyl-3,4-dihydro-1*H*-benzo[1,4]diazepine-2,5-dione (**15h**).

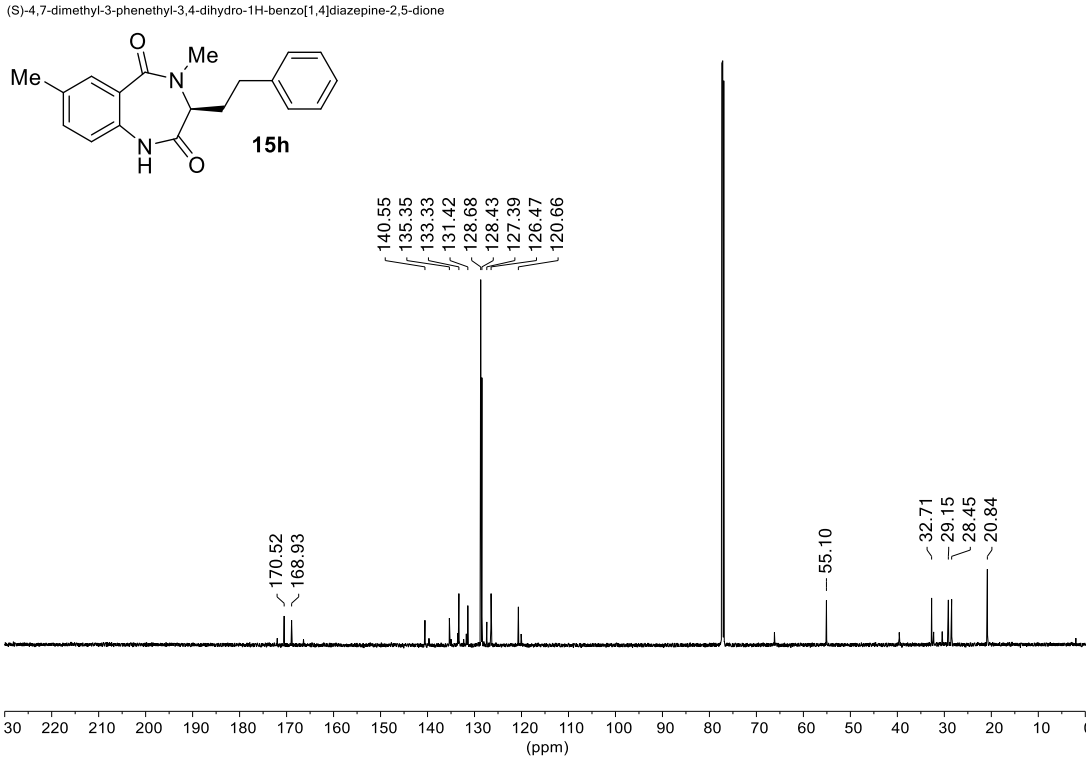

Figure S32. ^{13}C{^{1}H}-NMR spectrum (151 MHz) of (*S*)-4,7-dimethyl-3-phenethyl-3,4-dihydro-1*H*-benzo[1,4]diazepine-2,5-dione (**15h**).

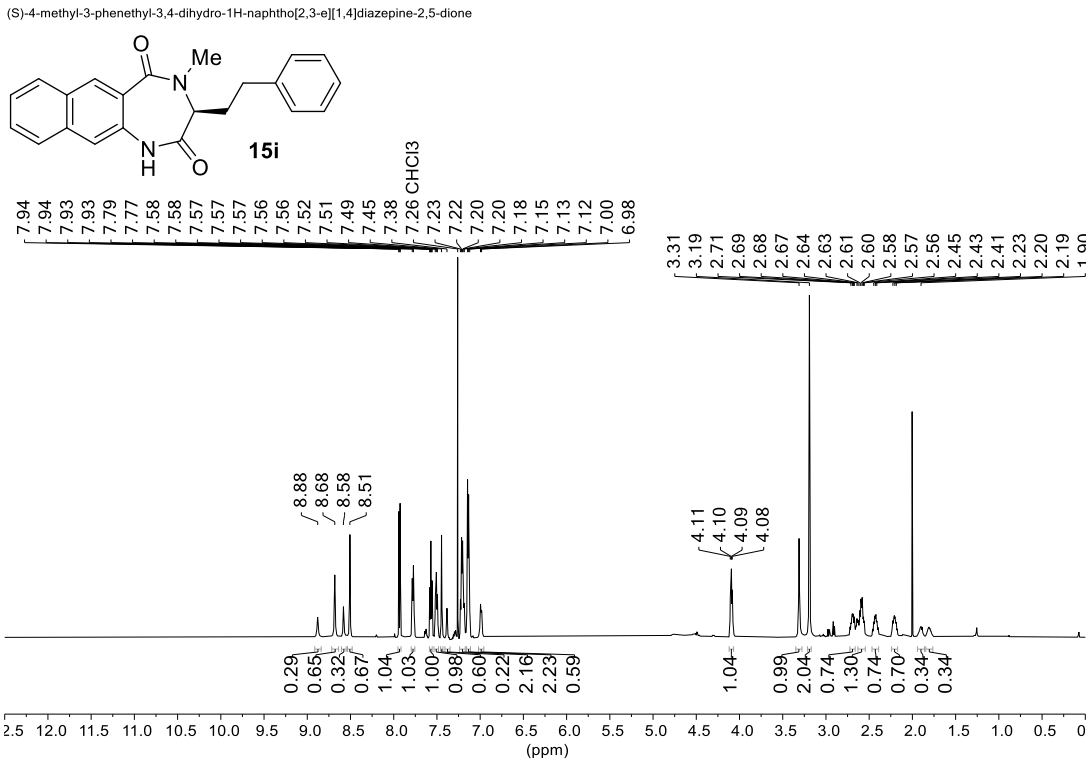

Figure S33. ^{1}H-NMR spectrum (600 MHz) of (*S*)-4-methyl-3-phenethyl-3,4-dihydro-1*H*-naphtho[2,3-*e*][1,4]diazepine-2,5-dione (**15i**).

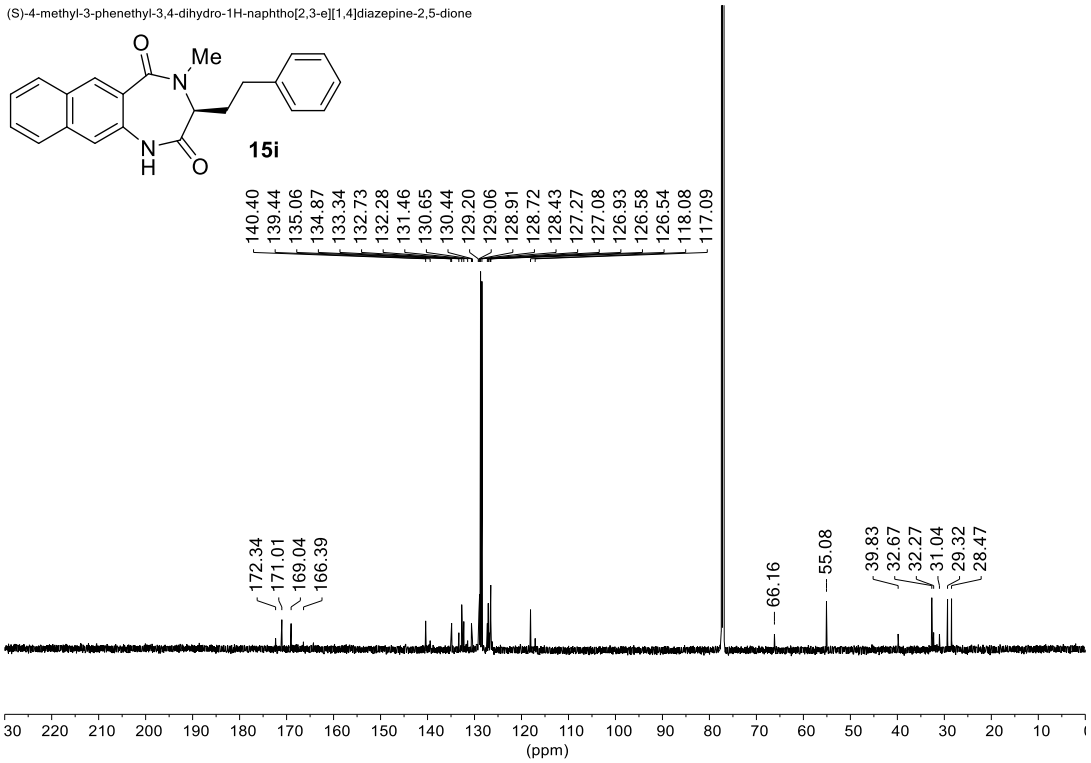

Figure S34. ^{13}C{^{1}H}-NMR spectrum (151 MHz) of (*S*)-4-methyl-3-phenethyl-3,4-dihydro-1*H*-naphtho[2,3-*e*][1,4]diazepine-2,5-dione (**15i**).

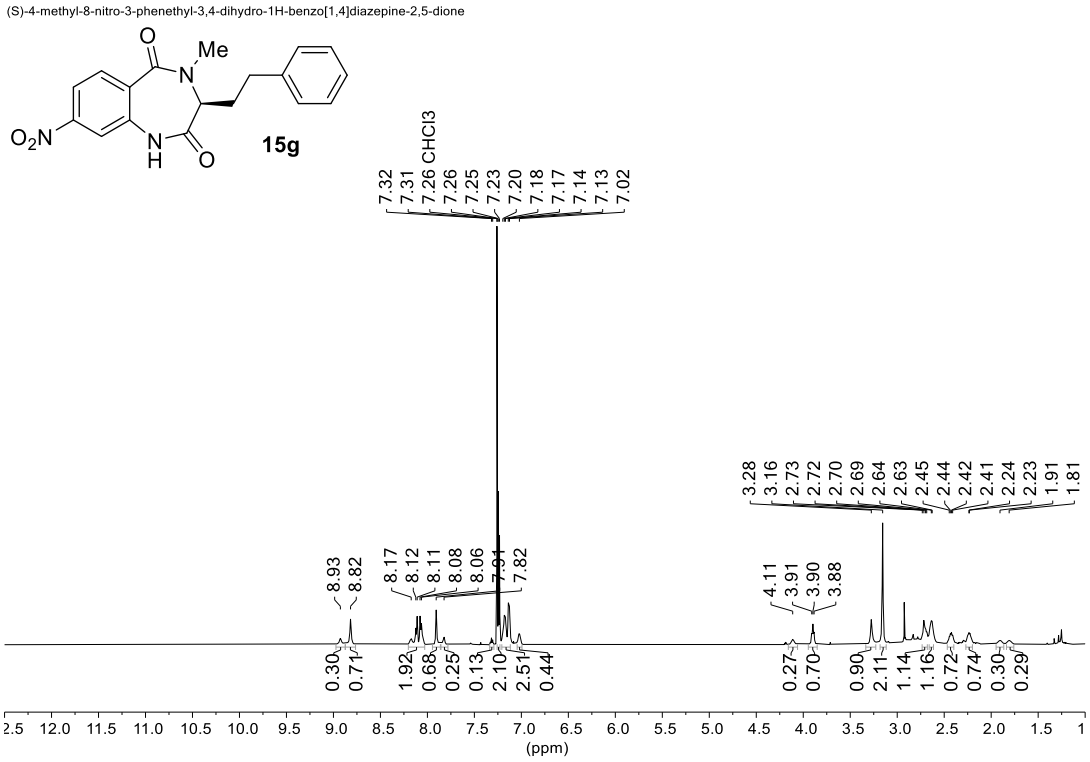

Figure S35. ^{1}H-NMR spectrum (600 MHz) of (*S*)-4-methyl-8-nitro-3-phenethyl-3,4-dihydro-1*H*-benzo[1,4]diazepine-2,5-dione (**15g**).

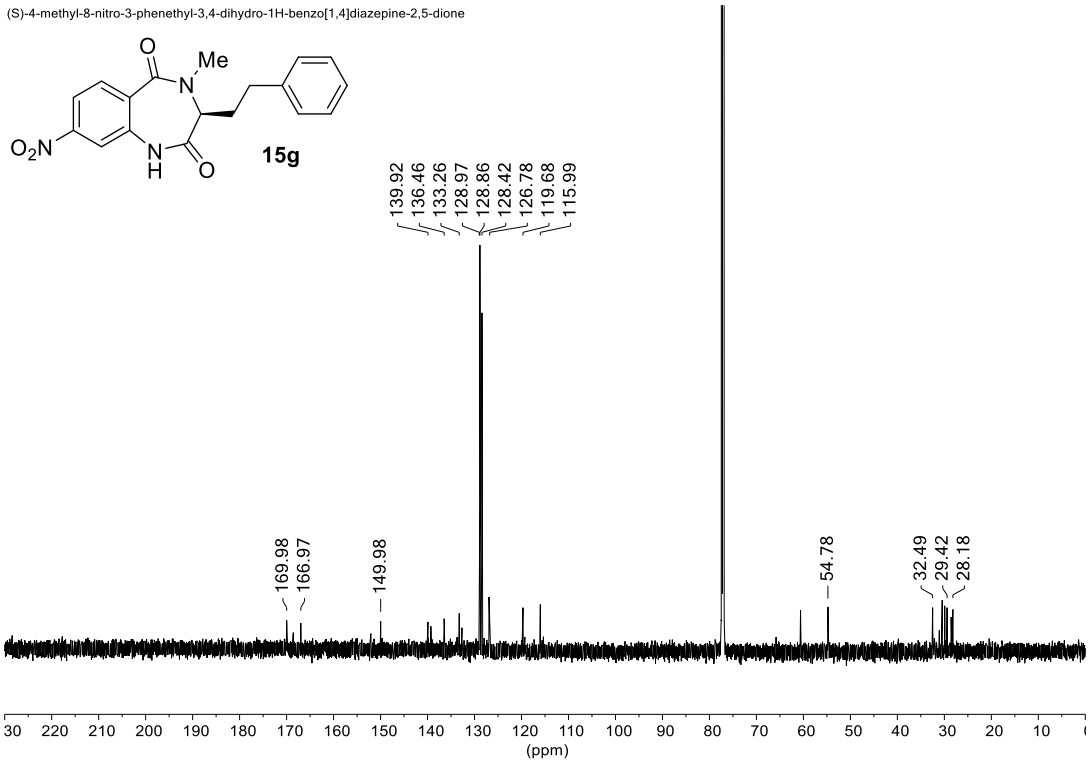

Figure S36. ^{13}C{^{1}H}-NMR spectrum (151 MHz) of (*S*)-4-methyl-8-nitro-3-phenethyl-3,4-dihydro-1*H*-benzo[1,4]diazepine-2,5-dione (**15g**).

5. Computational Studies

As a consequence of the hindered rotation about a single bond, the seven-membered 1,4-diazepine ring exists in the form of two atropisomers (**M** and **P**) with low rotational barrier (16–22 kcal/mol).[7-9] In compounds **5q**, **15a** and **15b** there is another chiral center at the C3 carbon atom (with S absolute configuration) which means that, based on the conformation of 1,4-diazepine ring, each compound can exist in the form of two diastereomers. In Figure S37 the diastereomers (labelled M and P, based on the configuration of 1,4 diazepine ring) of compound **15a** are shown.

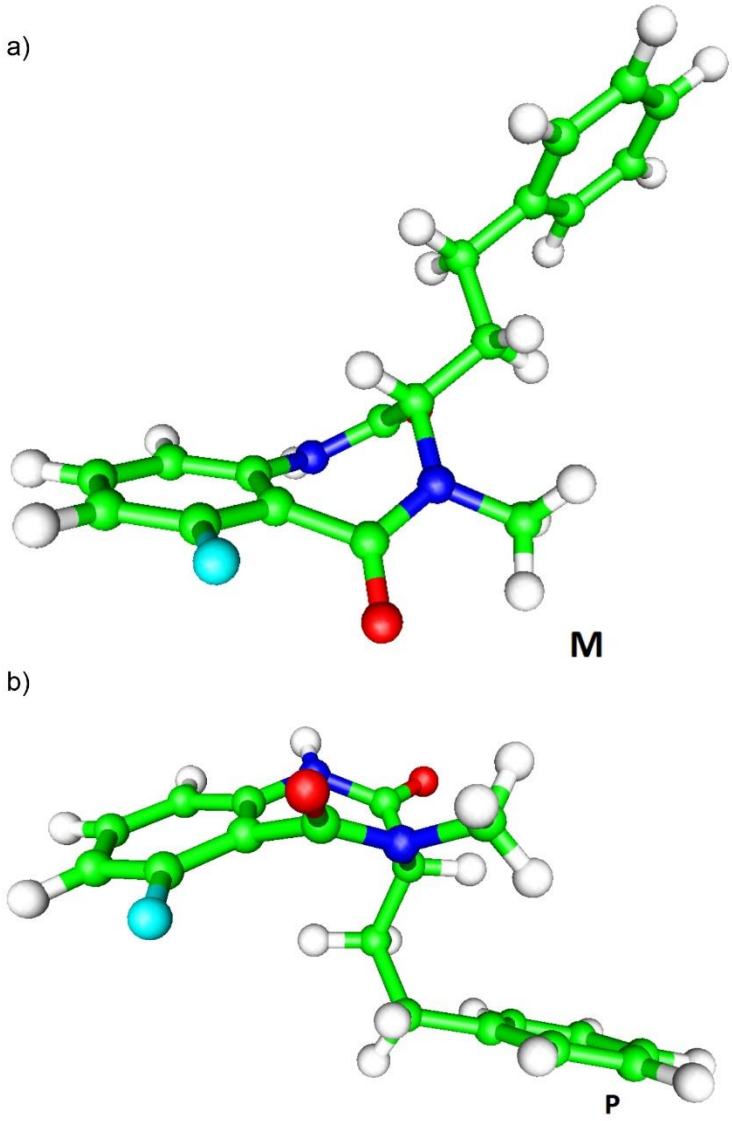

Figure S37. Diastereomers of compounds **15a**. Colour codes: carbon - green, hydrogen - white, nitrogen - blue, oxygen -red and fluorine - cyan.

The presence of two diastereomers was confirmed by ^{1}H NMR. Thus, inspecting the ^{1}H NMR spectrum of **5q** indicated the presence two diastereomers in slow exchange on the NMR time scale at room temperature (Figure S38). When the variable temperature ^{1}H NMR spectra were recorded, the coalescences of ^{1}H NMR signals at 8.6–8.4, 8.1–7.8, 7.1–6.9 and 4.2–3.8 ppm appeared. This phenomenon indicated that the simultaneous presence of both diastereomers in rapid exchange on the NMR time scale at elevated temperatures.

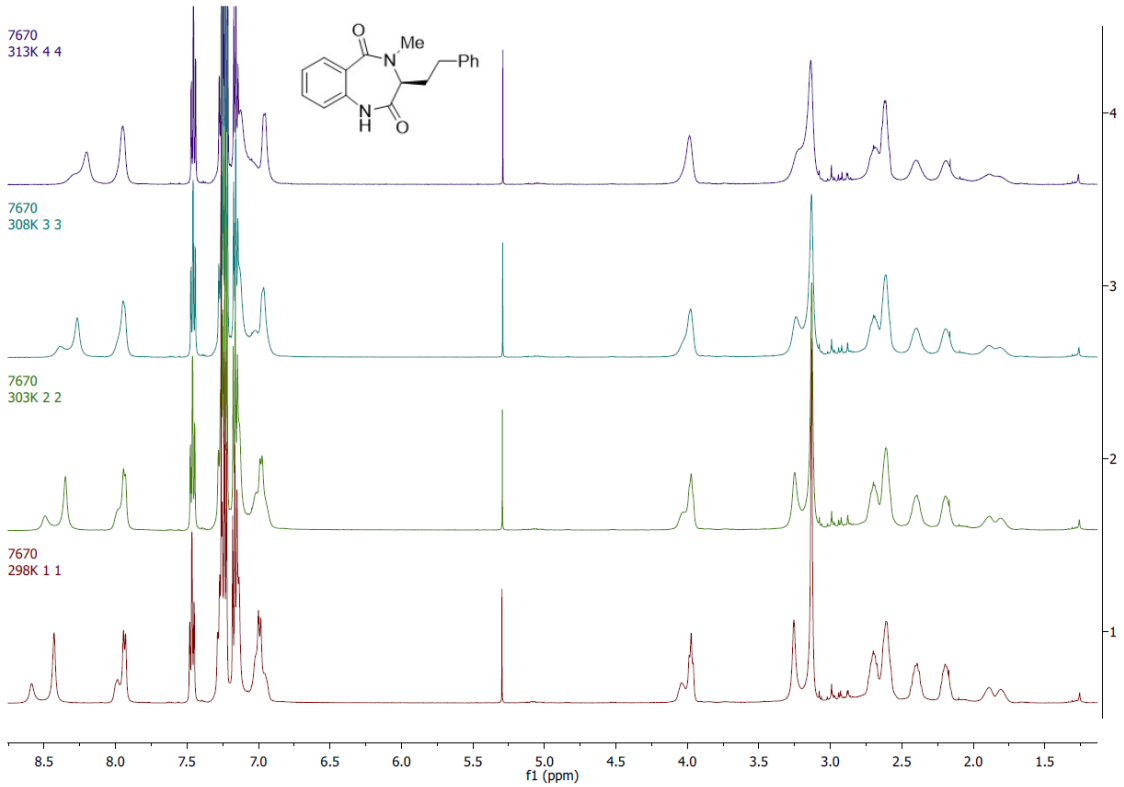

Figure S38. Variable temperature ^{1}H-NMR spectra of $CDCl_3$ solution of **5q** (400 MHz) at 298, 303, 308 and 313K.

DFT calculations

The geometry of diastereomers of all investigated compounds are fully optimised with DFT methods, at B3LYP/6-311G(d,p) level of theory and calculated energies are shown in Table S1. As indicated by DFT calculations, for all investigated compounds, M diastereomers are by 1.67 to 2.07 kcal/mol more stable than P diastereomers.

Table S1. Energies of M and P diastereomers of compounds **5q**, **15a** and **15b** calculated with B3LYP/6-311G(d,p) method.

Compound (diastereomer)	Energy (Hartree)	Relative energy (kcal/mol)
5q (M)	–956.983793	0.0
5q (P)	–956.9811363	1.67
15a (M)	–1056.2424077	0.0
15a (P)	–1056.2391112	2.07
15b (M)	–1056.2459547	0.0
15b (P)	–1056.2432769	1.68

Molecular docking

Since AutoDock Vina docking program is unable to simulate ring inversion, the separate docking study is conducted for each diastereomer. The results of the docking experiment are shown in Table S2. Binding energies are given as positive values, indicating attractive interactions.

Table S2. Highest binding energies (in kcal/mol) calculated by docking experiment.

Compound / Protein	**5q** (M)	**5q** (P)	**15a** (M)	**15a** (P)	**15b** (M)	**15b** (P)
LuxP	8.5	7.6	7.9	7.1	8.7	7.9
LasR	10.4	8.1	10.8	8.2	10.6	8.4
AbaI	8.6	7.7	8.9	7.8	8.9	8.0
RhlR	10.2	10.4	10.3	10.6	10.4	10.3

Results of the docking calculations clearly suggest that LasR and RhlR proteins are the most probable targets for binding investigated compounds, since the binding energies are about 2 kcal/mol higher than for LuxP and AbaI (Table S2). Also, LuxP, LasR and AbaI proteins show clear preference toward binding M diastereomeric form of investigated compounds, with calculated binding energies between 0.8 and 2.6 kcal/mol higher than for the P form (Table S2). On the other hand, the larger binding pocket of RhlR protein can accommodate both diastereomers with similar binding energies.

LuxP

For LuxP protein four potential binding sites were predicted for ligand binding with P2rank program (Figure S39a). The highest ranked binding site has P2rank score of 17.42 and ligand binding probability of 0.802. This binding site encompass autoinducer AI-2 binding pocket[10] and the best binding pose, found by our docking experiment for all investigated compounds (Figure S39b). Some residues from AI-2 binding pocket, including ASN-159, TRP-82 and GLN-77, are involved in van-der-Waals bonding interactions with investigated compounds (Figure S40 a–c). The orientations of all three docked compounds are almost the same with RMSD values less than 0.1 Å (Figure S39b). The only notable difference in binding mode of the three compounds is a new hydrogen bond formed between ARG-139 and fluorine atom of compound **15a** (Fig S40c).

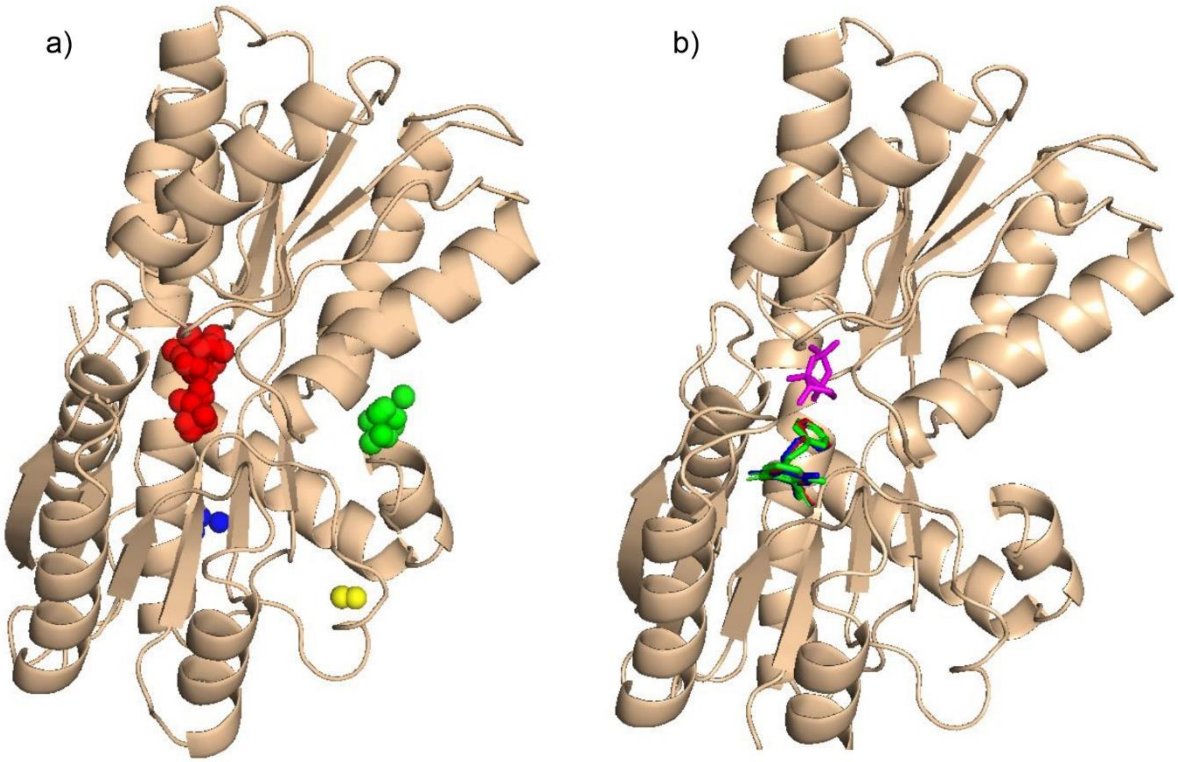

Figure S39. a) Potential ligand binding sites (LBS) in LuxP receptor predicted by P2rank program. Red spheres – LBS 1 (score=17.42, probability=0.802); Green spheres - LBS2 (score=6.36, probability=0.320); Blue spheres – LBS3 (score=1.69, probability=0.029); Yellow spheres – LBS4 (score=1.53, probability=0.023). b) The highest energy binding site for compounds **5q** (red), **15a** (blue) and **15b** (green) in LuxP. Magenta – autoinducer AI-2 from 1JX6 crystal structure of LuxP receptor.

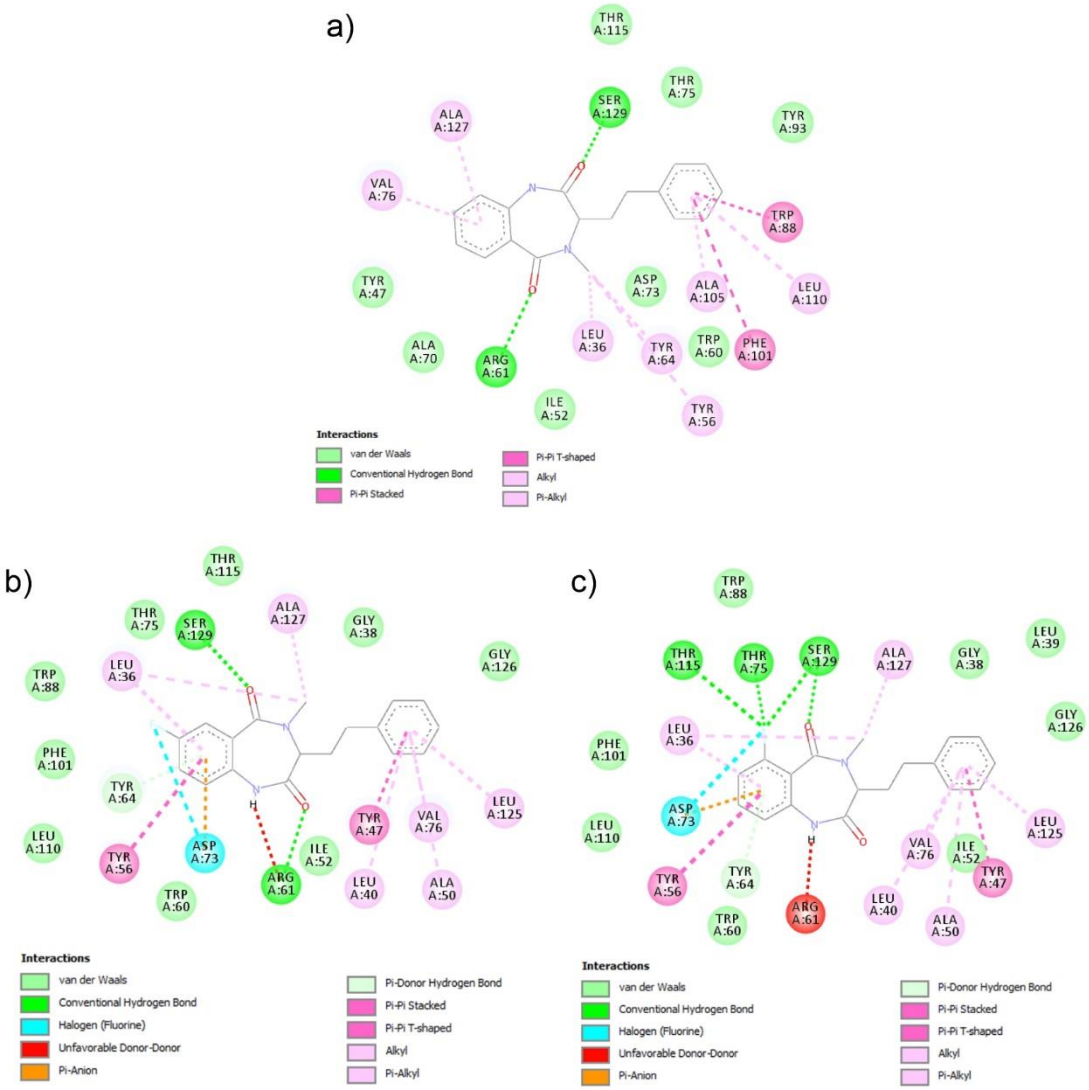

Figure S40. 2D diagram with labelled interactions between LuxP and compounds **5q** (a), **15a** (b) and **15b** (c).

LasR

Only one potential ligand binding site, known as autoinducer binding site, was predicted in LasR receptor (Figure S41a). In LasR crystal structure (PDB ID:6MVN) this iste is occupied with 3-oxo-*N*-[(3S)-2-oxotetrahydrofuran-3-yl] decanamide non-cognate autoinducer. In order to compare binding energies between this non-cognate autoinducer and our compounds a redocking study, with AutoDock Vina program, was done. AutoDock Vina successfully reproduced the binding site and ligand orientation for 3-oxo-*N*-[(3*S*)-2-oxotetrahydrofuran-3-yl] decanamide ligand with binding energy of 8.4 kcal/mol (Figure S41b).

In the highest energy binding site for compounds **15a** and **15b** there was an unfavourable donor-donor interaction between polar hydrogen atom from guanidino group of Arginine 61 and N–H group of the 1,4-diazepine ring (Figure 2c and d). In order to check the influence of this unfavourable contact on ligand binding the new flexible docking studies for compounds **15a** and **15b** with LasR receptor were conducted, where the side chain atoms of Arg 61 were allowed to rotate freely during docking run. The results of this flexible docking experiment produced the same orientation and the same binding energy for both ligands as with the rigid docking method (Figure S42). The only difference was observed in the orientation of Arg 61 side chain, in flexible docking it was slightly rotated out of the plane of the 1,4-diazepine ring, thus reducing the unfavourable donor-donor contact. As the consequence of this Arg 61 side chain movement, the hydrogen bond between Arg 61 and carbonyl oxygen from compound **15b** fell outside of criteria for Discovery Studio Visualizer software to recognise it (Figure S42b).

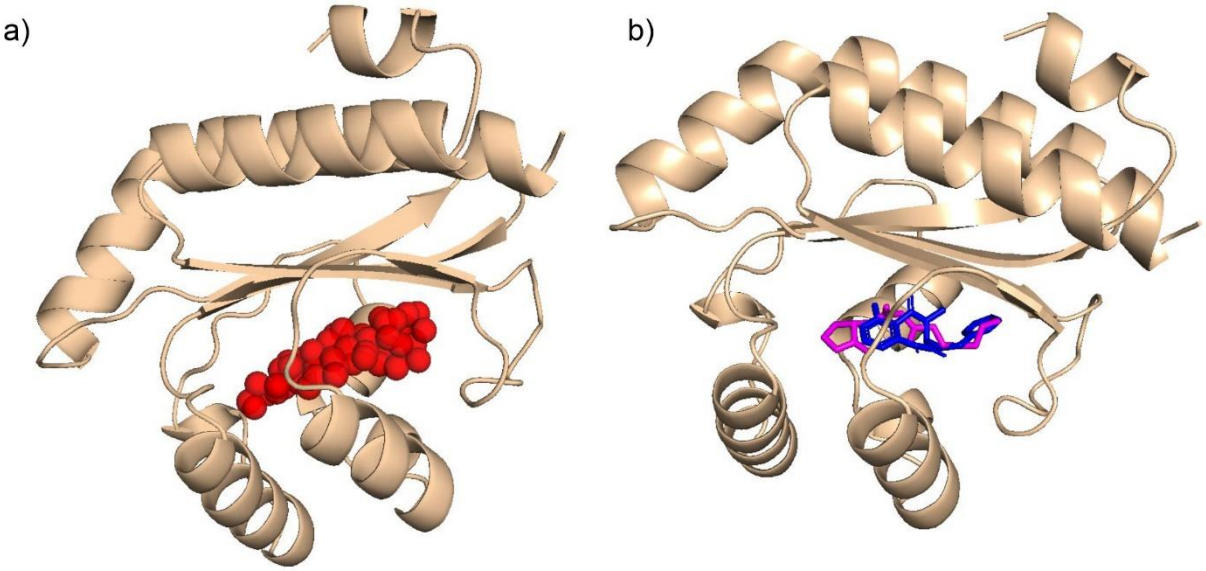

Figure S41. a) Potential ligand binding site (red spheres) in LasR protein predicted by P2rank program (score=27.70, probability=0.922) b) The highest energy binding site for compound **15a** (blue) and 3-oxo-*N*-[(3S)-2-oxotetrahydrofuran-3-yl] decanamide (magenta) non-cognate autoinducer (redocking experiment) in LasR autoinducer binding site.

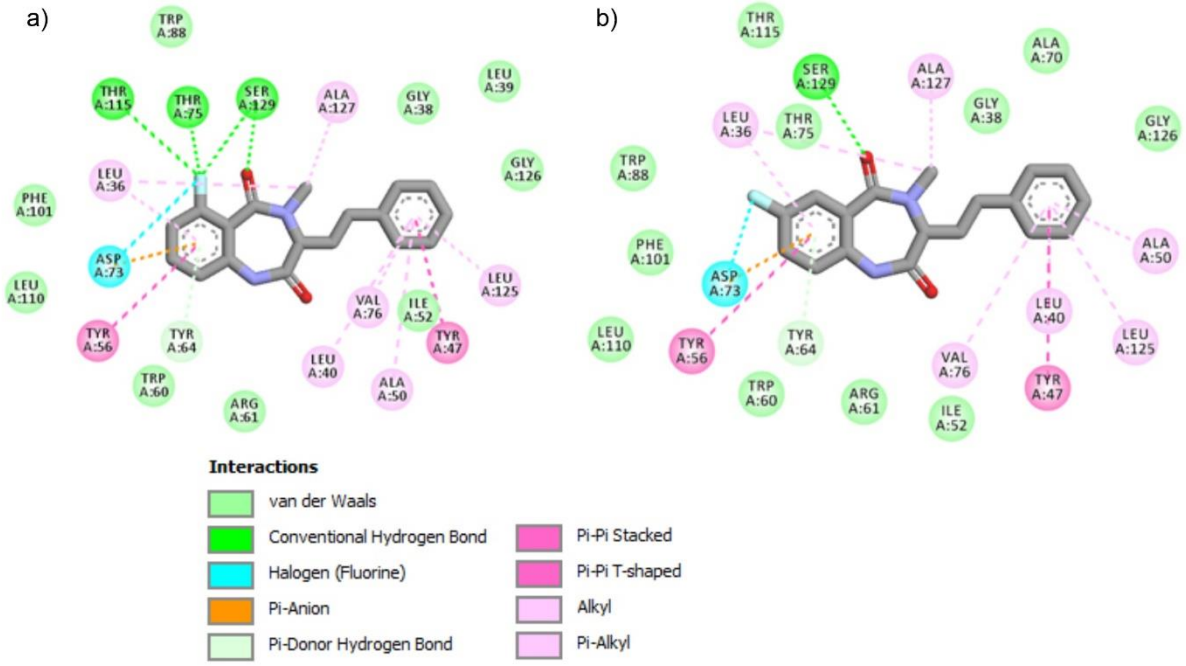

Figure S42. 2D diagram with labelled interactions, after flexible docking experiment, between compounds **15a** (a) and **15b** (b) and LasR receptor.

AbaI

Inhibitor-binding pocket and *S*-adenosyl methionine (SAM) binding site of AbaI receptor was predicted as the binding site for ligands with highest score (27.77) and probability (0.922) with P2rank program (Figure S43a). Previously, we identified inhibitor-binding pocket of AbaI receptor,[11] by docking the *N*-(3-oxocyclohex-1-en-1-yl)octanamide (J8-C8), a known inhibitor to Acyl-homoserine-lactone synthase proteins.[12] All investigated compounds bind to the inhibitor binding pocket of AbaI receptor, with estimated binding energies between 8.6 and 8.9 kcal/mol (for M diastereomer) and almost completely overlap with J8-C8 binding site (Figure S43b). The orientations of all three docked compounds are the same (Figure S43b). For compounds **15a** and **15b**, no interactions between fluorine atom and protein residues in the active site were found (Figure S44 b,c).

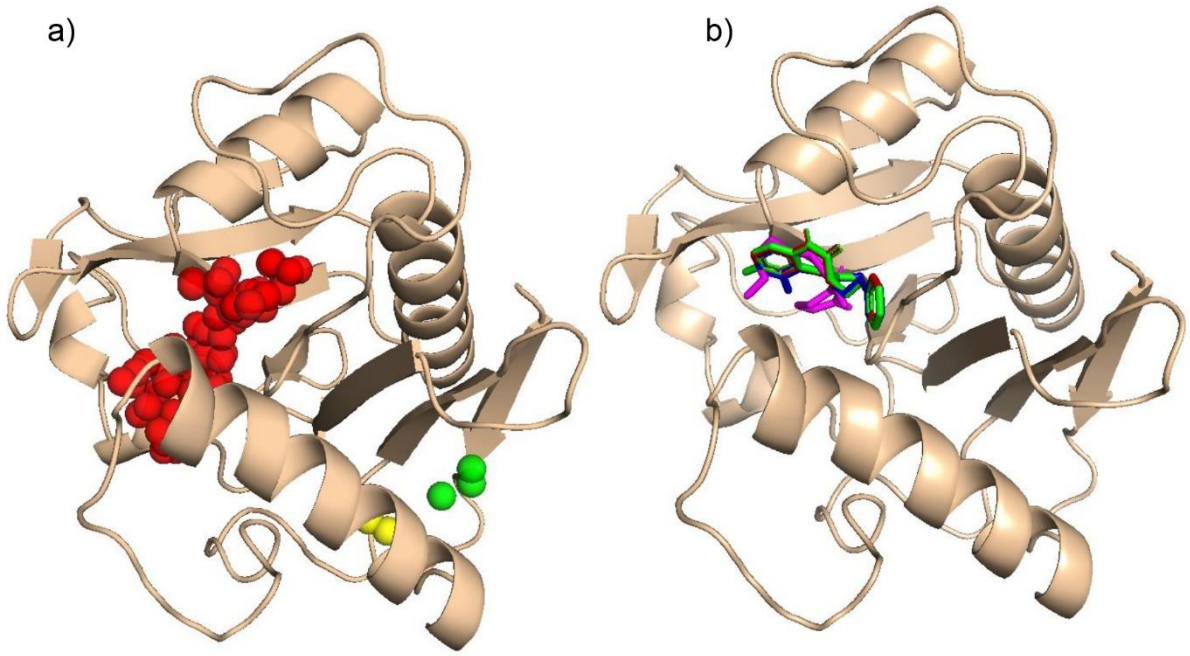

Figure S43. a) Potential ligand binding sites (LBS) in AbaI protein predicted by P2rank program. Red spheres – LBS 1 (score=27.77, probability=0.922); Green spheres - LBS2 (score=2.10, probability=0.048); Yellow spheres – LBS3 (score=1.48, probability=0.021). b) The highest energy binding site for compounds **5q** (red), **15a** (blue) and **15b** (green) in AbaI. Magenta – binding site of *N*-(3-oxocyclohex-1-en-1-yl)octanamide (J8-C8) inhibitor found in our previous study.[11]

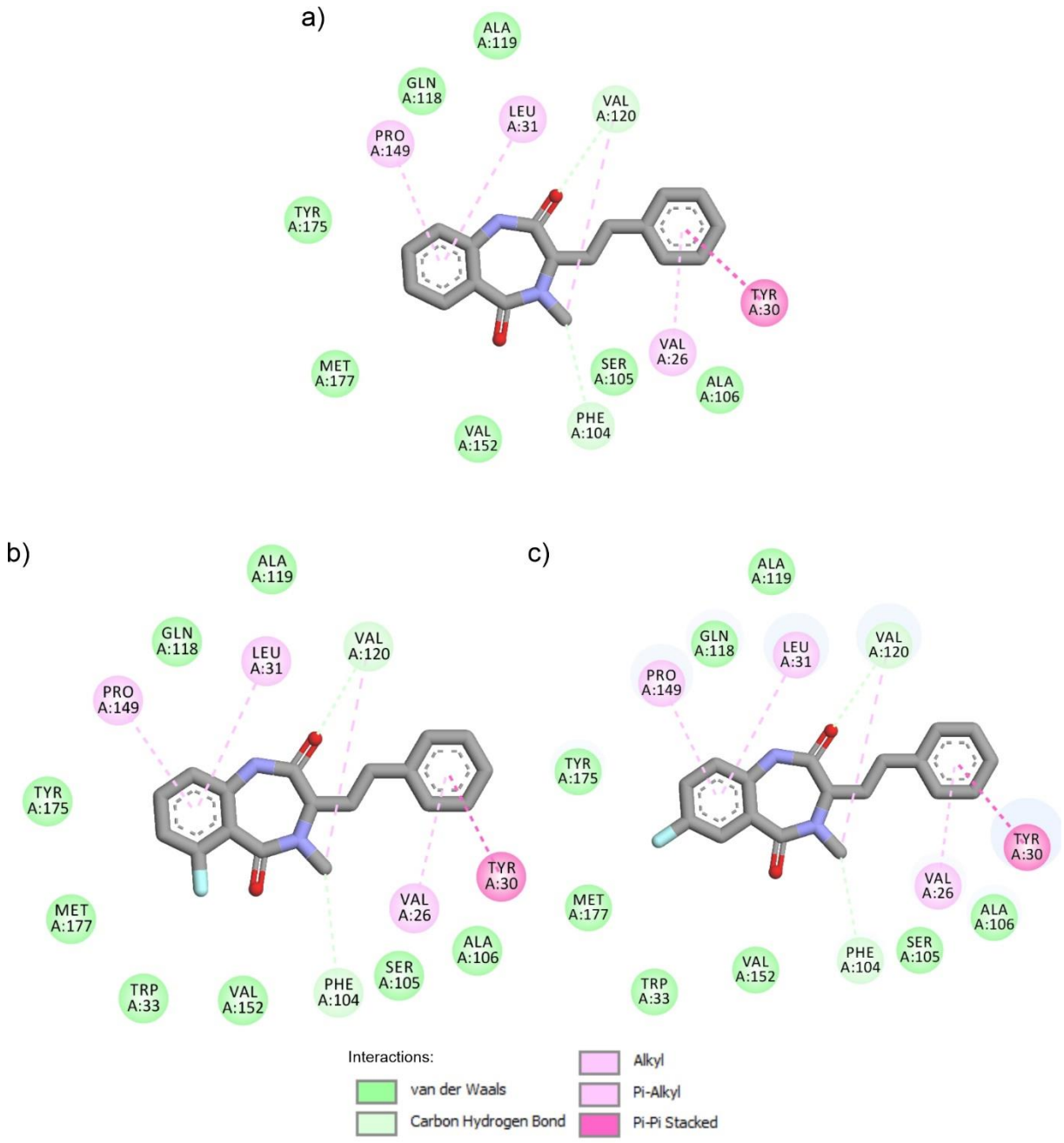

Figure S44. 2D diagram with labelled interactions between AbaI and compounds **5q** (a), **15a** (b) and **15b** (c).

RhlR

The calculated binding energies of compounds **5q**, **15a** and **15b** to RhlR are much higher than to LuxP and AbaI proteins, and of the similar magnitude to LasR (Table S2). This makes RhlR the second most probable binding target for investigated compounds. From four potential ligand binding sites identified by P2rank program (Figure S45a) only first one can bind to the investigated compounds with significant binding energy (Figure S45b).

Again, in this receptor all three ligands are oriented in the same way and there is no difference in interactions with the protein residues (Fig. S45b). Recently,[13] 1-(3,4-Difluorophenyl)hex-1-yn-3-one was identified as a very potent RhlR antagonist by the docking study. Our redocking experiment found the same high affinity docking site of 1-(3,4-Difluorophenyl)hex-1-yn-3-one and with the same ligand orientation,[11] as reported in the original study[13] (Figure S45b), but with significantly lower binding energy (8.5 kcal/mol) than compounds **5q**, **15a** and **15b** (from 10.2 to 10.6 kcal/mol). This can indicate that compounds **5q**, **15a** and **15b** are potentially better RhlR inhibitors then 1-(3,4-Difluorophenyl)hex-1-yn-3-one. Interestingly, in both docking experiments with fluorinated compounds (the ones presented in this study as well as in the earlier study),[13] no interactions between fluorine atom(s) from the substances and amino acid residues from RhlR are found (Figure S46).

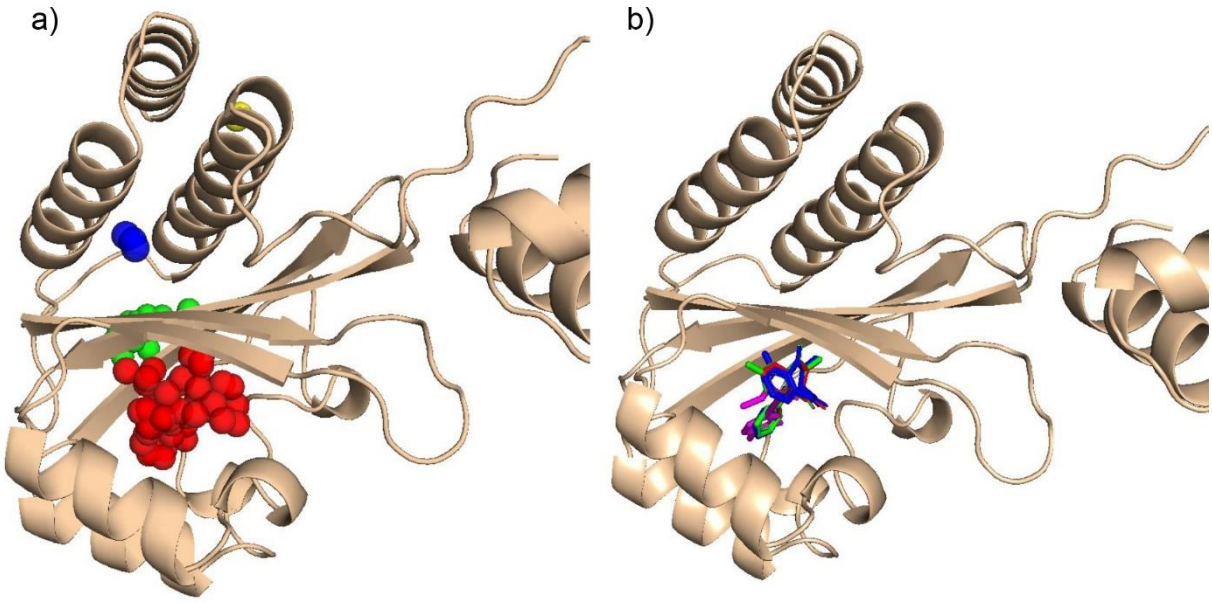

Figure S45. a) Potential ligand binding sites (LBS) in RhlR receptor predicted by P2rank program. Red spheres – LBS 1 (score=34.38, probability=0.950); Green spheres - LBS2 (score=5.49, probability=0.262); Blue spheres – LBS3 (score=1.73, probability=0.031); Yellow spheres – LBS4 (score=1.38, probability=0.017). b) The highest energy binding site for compounds **5q** (red), **15a** (blue) and **15b** (green) in RhlR receptor. Magenta – binding site of 1-(3,4-Difluorophenyl)hex-1-yn-3-one antagonist found in our previous study.

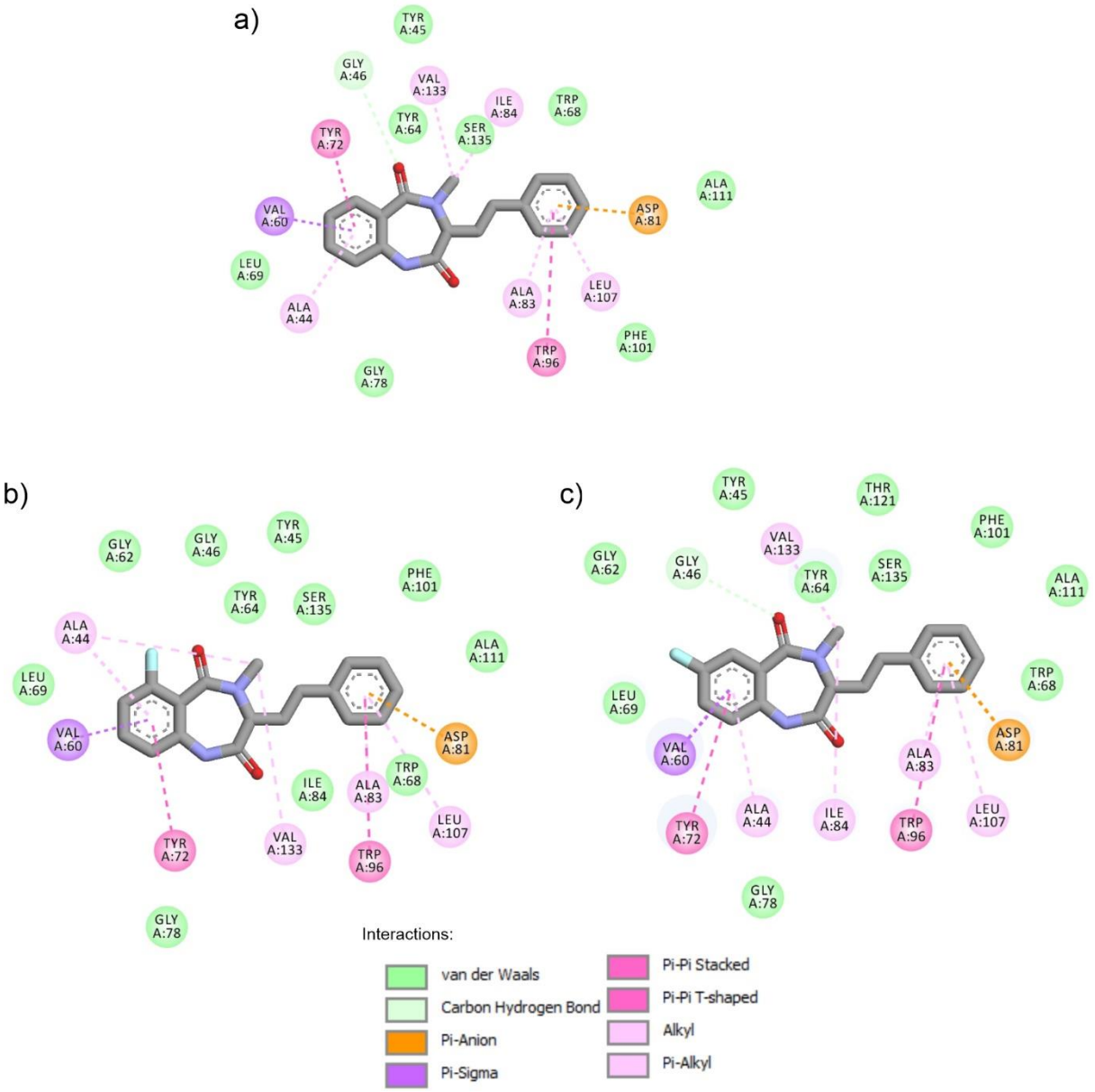

Figure S46. 2D diagram with labelled interactions between RhlR and compounds **5q** (a), **15a** (b) and **15b** (c).

The stability of protein-ligand complexes for LasR protein (molecular dynamics simulations)

Amber (version 24)[14,15] software with GPU support was used for molecular dynamics simulations and AmberTools (version 23)[16] suite of programs was used for protein and ligand preparation and analysis of the results. The initial structure for the protein-ligand complexes was taken from docking calculations. For the LasR protein, standard ff19SB protein force field[17] was chosen, and ligands bonding and Lennard-Jones parameters were taken from General Amber Force Field (gaff2).[18] For ligand atoms partial charges, first Merz-Singh-Kollman Electrostatic Potentials were calculated at MP2/aug-cc-pVTZ level of theory, then atomic partial charges were calculated using RESP algorithm[19] with PyRESP program.[20] Protein-ligand complex was solvated in a truncated-octahedron box (dimensions 69.214 × 69.214 × 69.214 Å, total volume 255251.7 Å^3) using OPC 4 point water model,[21] and periodic boundary conditions (PBC) were set. The system was initially minimised for 2000 steps using the Newton-Raphson algorithm, and then slowly heated from 100 K to 298 K for 1 ns with a time-step of 1 fs, while keeping the volume constant. The initial restraint on protein and ligand atoms was 100 kcal/mol-Å^2. Next, the system was relaxed for a total of 6 ns with 1 fs time step, in NPT ensemble, by slowly lifting restraints (to 10.0, 1.0, and 0.1 kcal/mol-Å^2) on protein and ligand atoms. Finally, 5 ns of equilibration in an NPT ensemble with 1 fs time step and no restraints was conducted. For the 100 ns production run, the NPT ensemble was chosen with Langevin thermostat and Berendsen barostat and 2 fs time step. SHAKE algorithm was employed to impose constraints on hydrogen atoms. RMSD analysis of molecular dynamics trajectories was conducted with cpptraj program.[22] During the production run of molecular dynamics simulations, the core of the LasR protein remained stable with most of the movement in the *C*- and *N*-terminal regions and loops connecting β-sheets and α-helices. In all three simulations, the total RMSD value for protein atoms did not exceed 3 Å (Figure S47).

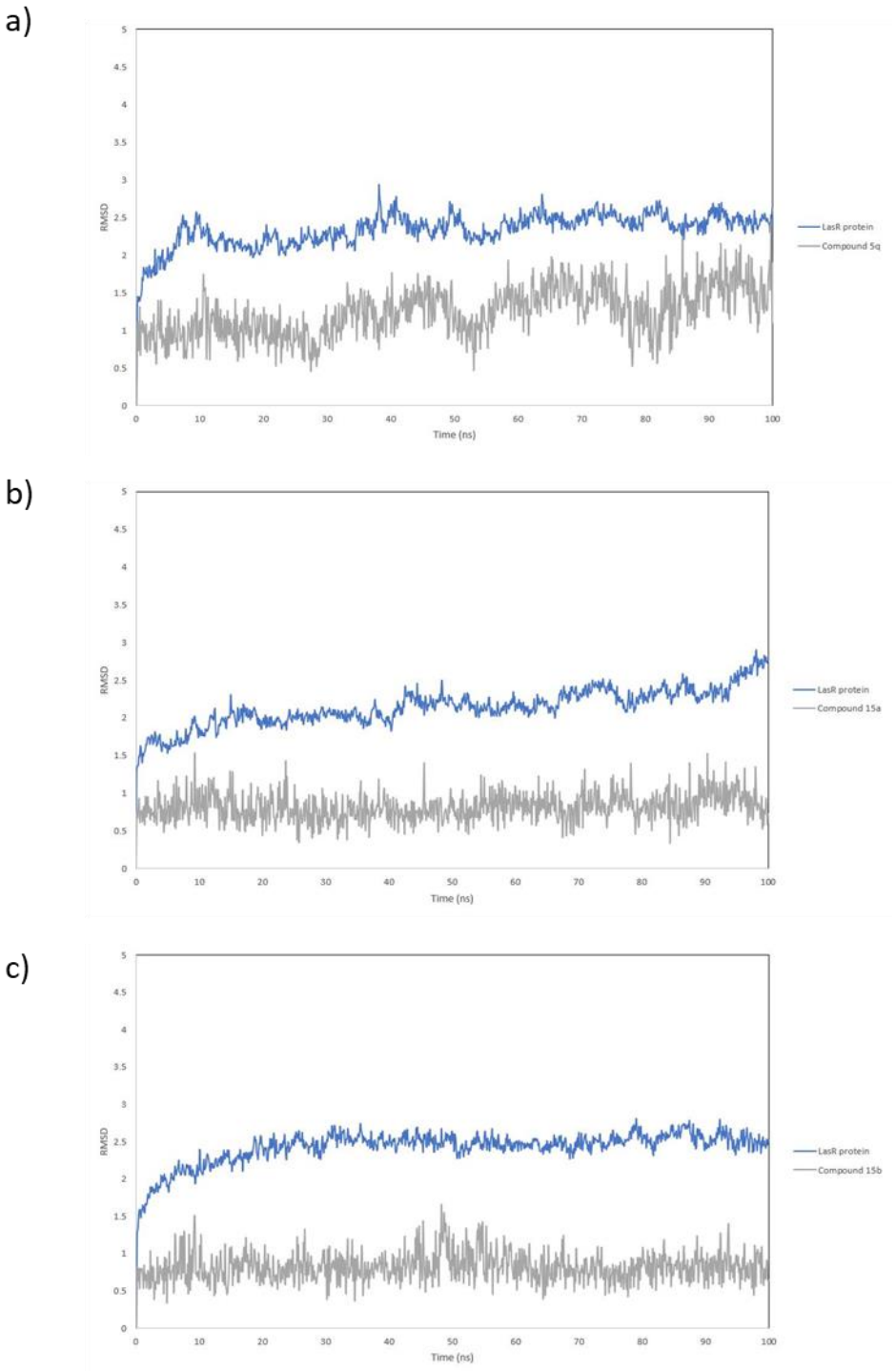

Figure S47. RMSD for protein and ligand from molecular dynamics simulations for a) compound **5q**, b) compound **15a**, and c) compound **15b**.

Even less movement was found for the ligand atoms. All three investigated compounds kept their orientation in the LasR autoinducer binding pocket found by the initial docking experiments. Most of the movement of ligand atoms was found in the phenethyl part of the molecule, while the benzo[1,4]diazepine-2,5-dione part of the molecule remained rigid during the production run. In Figure S48 the differences in ligand position at the beginning and the end of the production run of molecular dynamics simulation for all three investigated compounds are shown.

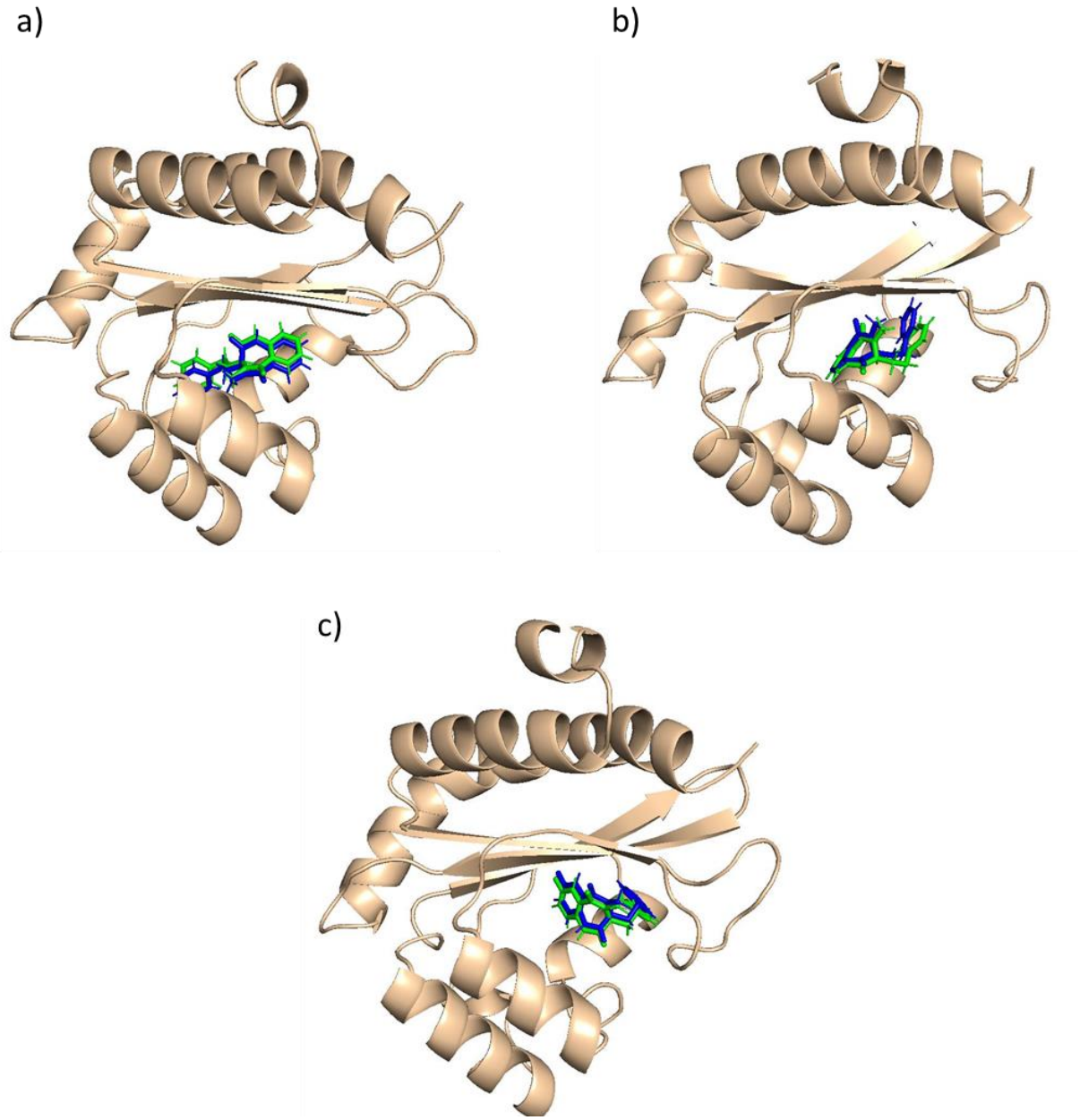

Figure S48. The differences in ligand orientation in the LasR autoinducer binding pocket for a) compound **5q**, b) compound **15a**, and c) compound **15b** at the beginning (green) and at the end (blue) of the molecular dynamics 100 ns production run.

6. References

1. C. P. Rosenau, B. J. Jelier, A. D. Gossert and A. Togni, *Angew. Chem. Int. Ed.*, 2018, **57**, 9528–9533.
2. R. S. Blosser and K. M. Gray, *J. Microbiol. Meth.*, 2000, **40**, 47–55.
3. M. Einsiedler, C. S. Jamieson, M. A. Maskeri, K. N. Houk and T. A. M. Gulder, *Angew. Chem. Int. Ed.*, 2021, **60**, 8297–8302.
4. M. Einsiedler and T. A. M. Gulder, *Nat. Commun.*, 2023, **14**, 3658.
5. M. A. Blaskovich and M. Kahn, *Synthesis*, 1998, **30**, 379–380.
6. J. P. Mayer, J. Zhang, K. Bjergarde, D. M. Lenz and J. J. Gaudino, *Tetrahedron Lett.*, 1996, **37**, 8081–8084.
7. B. Paizs and M. Simonyi, *Chirality*, 1999, **11**, 651–658.
8. N. W. Gilman, P. Rosen, J. V. Earley, C. Cook and L. J. Todaro, *J. Am. Chem. Soc.*, 1990, **112**, 3969–3978.
9. P. C. H. Lam and P. R. Carlier, *J. Org. Chem.*, 2005, **70**, 1530–1538.
10. X. Chen, S. Schauder, N. Potier, A. Van Dorsselaer, I. Pelczer, B. L. Bassler and F. M. Hughson, *Nature*, 2002, **415**, 545–549.
11. S. S. Bogojevic, D. Perminova, J. Jaksic, M. Milcic, V. Medakovic, J. Milovanovic, J. Nikodinovic-Runic and V. Maslak, *J. Mol. Struct.*, 2024, **1300**, 137291.
12. J. Chung, E. Goo, S. Yu, O. Choi, J. Lee, J. Kim, H. Kim, J. Igarashi, H. Suga, J. S. Moon, I. Hwang and S. Rhee, *Proc. Natl. Acad. Sci. USA*, 2011, **108**, 12089–12094.
13. S. Nam, S.-Y. Ham, H. Kwon, H.-S. Kim, S. Moon, J.-H. Lee, T. Lim, S.-H. Son, H.-D. Park and Y. Byun, *J. Med. Chem.*, 2020, **63**, 8388–8407.
14. D. A. Case, H. M. Aktulga, K. Belfon, I. Y. Ben-Shalom, J. T. Berryman, S. R. Brozell, D. S. Cerutti, T. E. Cheatham, III, G. A. Cisneros, V. W. D. Cruzeiro, T. A. Darden, N. Forouzesh, M. Ghazimirsaeed, G. Giambaşu, T. Giese, M. K. Gilson, H. Gohlke, A. W. Goetz, J. Harris, Z. Huang, S. Izadi, S. A. Izmailov, K. Kasavajhala, M. C. Kaymak, A. Kovalenko, T. Kurtzman, T. S. Lee, P. Li, Z. Li, C. Lin, J. Liu, T. Luchko, R. Luo, M. Machado, M. Manathunga, K. M. Merz, Y. Miao, O. Mikhailovskii, G. Monard, H. Nguyen, K. A. O'Hearn, A. Onufriev, F. Pan, S. Pantano, A. Rahnamoun, D. R. Roe, A. Roitberg, C. Sagui, S. Schott-Verdugo, A. Shajan, J. Shen, C. L. Simmerling, N. R. Skrynnikov, J. Smith, J. Swails, R. C. Walker, J. Wang, J. Wang, X. Wu, Y. Wu, Y. Xiong, Y. Xue, D. M. York, C. Zhao, Q. Zhu, and P. A. Kollman, Amber 2024, University of California, San Francisco, CA, 2024.
15. R. Salomon-Ferrer, A. W. Goetz, D. Poole, S. Le Grand, and R. C. Walker, *J. Chem. Theory Comput*., 2013, **9**, 3878–3888.
16. D. A. Case, H. M. Aktulga, K. Belfon, D. S. Cerutti, G. A. Cisneros, V. W. D. Cruzeiro, N. Forouzesh, T. J. Giese, A. W. Götz, H. Gohlke, S. Izadi, K. Kasavajhala, M. C. Kaymak, E. King, T. Kurtzman, T.-S. Lee, P. Li, J. Liu, T. Luchko, R. Luo, M. Manathunga, M. R. Machado, H. M. Nguyen, K. A. O'Hearn, A. V. Onufriev, F. Pan, S. Pantano, R. Qi, A. Rahnamoun, A. Risheh, S. Schott-Verdugo, A. Shajan, J. Swails, J. Wang, H. Wei, X. Wu, Y. Wu, S. Zhang, S. Zhao, Q. Zhu, T. E. Cheatham III, D. R. Roe, A. Roitberg, C. Simmerling, D. M. York, M. C. Nagan, K. M. Merz Jr., *J. Chem. Inf. Model.*, 2023, **63**, 6183–6191.
17. C. Tian, K. Kasavajhala, K. A. A. Belfon, L. Raguette, H. Huang, A. N. Migues, J. Bickel, Y. Wang, J. Pincay, Q. Wu and C. Simmerling, *J. Chem. Theory Comput.*, 2019, **16**, 528–552.
18. J. Wang, R. M. Wolf, J. W. Caldwell, P. A. Kollman, D. A. Case, *J. Comput. Chem.*, 2004, **25**, 1157–1174.
19. C. I. Bayly, P. Ciepak, W. D. Ciepak, P. A. Kollman, *J. Phys. Chem.,* 1993, **97**, 10269–10280.
20. S. Zhao, H. Wei, P. Cieplak, Y. Duan, R. Luo, *J. Chem. Theory Comput.,* 2022, **18**, 6, 3654–3670.
21. S. Izadi, R. Anandakrishnan, A. V. Onufriev, *J. Phys. Chem. Lett.,* 2014, **5**, 3863–3871.
22. D. R. Roe, T. E. Cheatham III, *J. Chem. Theory Comput.*, 2013, **9**, 3084–3095.